Theoretical Studies of Transport at the Nanoscale

A Thesis

Submitted in partial fulfillment for the Degree of

Master of Science

as a part of Integrated Ph.D. programme in

Materials Science

by

Sudeshna Sen

Chemistry and Physics of Materials Unit
Jawaharlal Nehru Centre for Advanced Scientific Research
Bangalore – 560 064

MARCH 2011

To Ma and Baba

DECLARATION

I hereby declare that the matter embodied in the thesis entitled "**Theoretical Studies of Transport at the Nanoscale**" is the result of investigations carried out by me at the Chemistry and Physics of Materials Unit, Jawaharlal Nehru Centre for Advanced Scientific Research, Bangalore, India under the supervision of Dr. N. S. Vidhyadhiraja and that it has not been submitted elsewhere for the award of any degree or diploma.

In keeping with the general practice in reporting scientific observations, due acknowledgement has been made whenever the work described is based on the findings of other investigators.

Sudeshna Sen

CERTIFICATE

I hereby certify that the matter embodied in this thesis entitled "**Theoretical Studies of Transport at the Nanoscale**" has been carried out by Ms. Sudeshna Sen at the Chemistry and Physics of Materials Unit, Jawaharlal Nehru Centre for Advanced Scientific Research, Bangalore, India under my supervision and that it has not been submitted elsewhere for the award of any degree or diploma.

Dr. N. S. Vidhyadhiraja
(Research Supervisor)

Acknowledgements

Even though it is only my name that appears on the cover page of this thesis, many people have contributed to the work presented here. I am grateful to each one of them.

First of all, I would like to thank my advisor Dr. N. S. Vidhyadhiraja, who had not just been a guide to me in the academics but also in many other aspects. I thank you very much, Sir, for being my guardian when my parents are not with me. From the academics point of view, he is an inspiring figure from many directions. He taught me to be optimistic, patient and most importantly think of my own and try to be thourough in all my concepts. He makes physics so very interesting!

I would like to thank all my course intructors starting from my university days. I really owe to them for whatever I am now. I would like to thank Prof. Balasubramanian, for making computation exciting, Prof. Kulkarni for helping me improve my attitude towards science and my presentation skills, Prof. Shobhana Narasimhan for making my Solid State Physics concepts clearer. And also Prof. Chandrabhas Narayana for always encouraging me

with his smiling face.

I thank my labmates, especially, Himadri da and Dasari for all our scientific discussions and making the office ambience pleasant and suitable for research. I also thank Anubhab da from EMU for helping me with the MATLAB codes.

Last but not the least, I wish to thank my parents above all, because, without their constant encouragement and loving support any study would not have been possible. **Thank you Ma and Baba**.

Contents

List of Figures

Chapter 1

Introduction

This dissertation is about electronic transport in nanoscale conductors. Nanotechnology and nanophysics are contemporary and emerging areas and that is because of the ineteresting features that emerge as one explores smaller and smaller length scales. These are subfields of condensed matter physics with a focus on electrical transport phenomena occurring at nanoscale dimensions, and, hence quantum mechanics plays an important role.

Nanoscience deals with the study of systems whose size in atleast one of the dimensions is less than 100 nm(1 nm= 10^{-9} m): for example a carbon nanotube device has its radius of the order of 5 nm while length of the order of 0.5 μm. Depending on the temperature, interaction etc., nano dimensions can incorporate different effects. Especially, quantum effects become inevitable in these systems. Depending on the operational length scales different effects become dominant. Figure (1.1) is a concise image showing the relevant length scales with examples of micro-, meso-, and macrosystems.

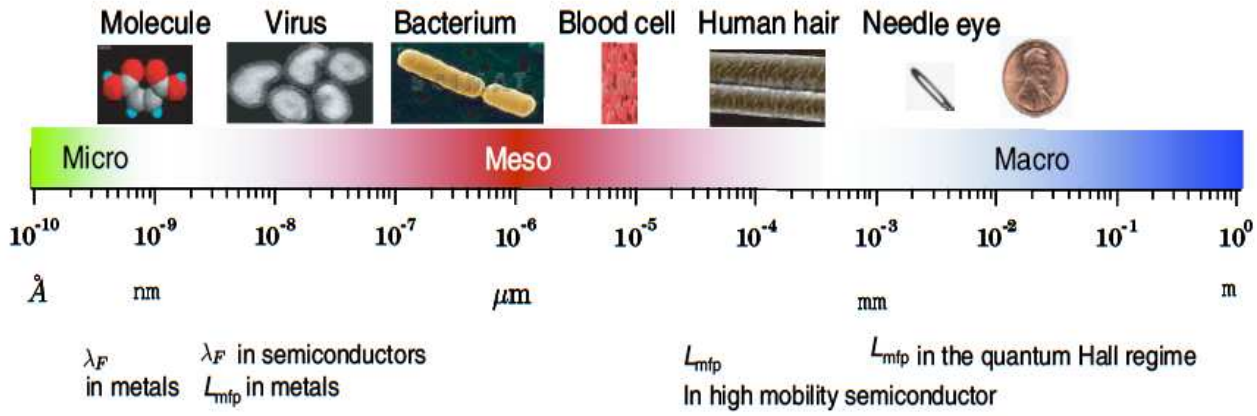

Figure 1.1: Zone of micro-, meso-, and macrosystems.

1.1 Nanoscale Conductors

Nanoscale conductors exhibit subtle and sophisticated phenomena which are deeply rooted in quantum mechanics. Figure (1.2) shows typical nanoscale systems of present interest. These include nanotubes or long atomic wires in contact with metal electrodes [2, 12] (figure (1.2), left panel) and a narrow channel or electron waveguides [1] sandwiched between bulk metals (figure (1.2), right panel).

The main classification of system dimension is achieved by the comparison between the physical length and the Fermi wavelength. Fermi wavelength, λ_F, is defined as the wavelength of the carriers at the Fermi level; $\lambda_F = 2\pi/k_F$; k_F being the Fermi momentum. Conduction in any system is dominated by electrons at the Fermi level; λ_F, therefore represents the wavelength of the major carriers. λ_F in metals is typically of atomic dimension ($\sim$Å), whereas in semiconductors it is of about $10 - 100$ nm. Suppose L_x, L_y, L_z represent the physical length of a system satisfying $L_x < L_y < L_z$. Table (1.1) represents the condition of each dimension

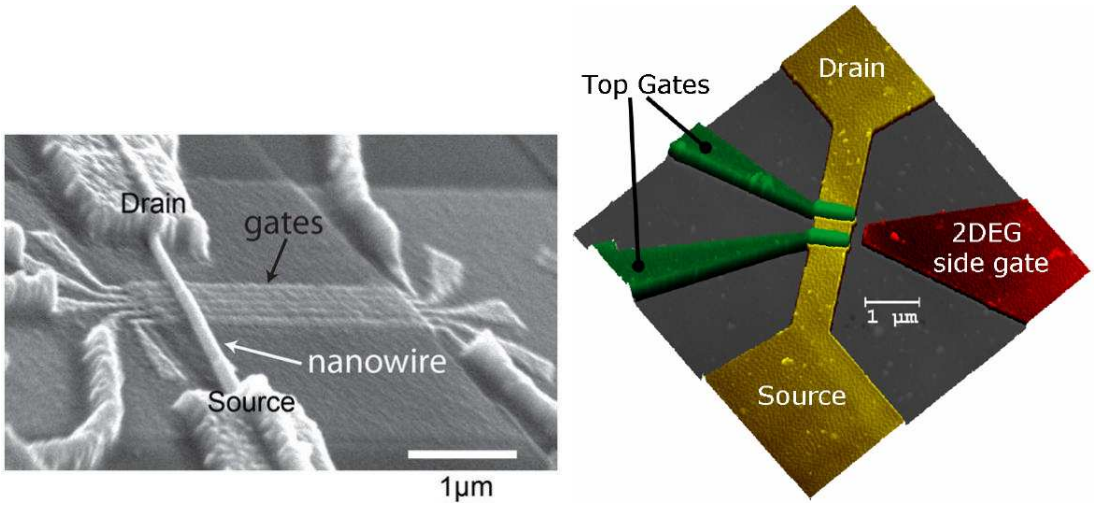

Figure 1.2: Recent experimental set ups consisting of a nanowire (left) and a 2DEG quantum dot (right). Credit: (Left)Image courtesy of Delft University of Technology [2]; credit: (right)image courtesy Slinker *et. al.* of University of Wisconsin [1].

relevant to different length scales.

Table 1.1: Dimensions according to length scales in mesoscopic systems.

Dimension	Condition
One	$L_x,\ L_y\ <\ \lambda_F\ <\ L_z$
Two	$\lambda_F\ \sim\ L_x\ <<\ L_y,\ L_z$
Three	$\lambda_F\ <<\ L_x,\ L_y\ L_z$

An important observation in nanoscale systems is the quantization of conductance. Early experiments [4, 5, 6, 7, 8] show this feature which was first predicted theoretically by Landauer [3]. Figure (1.3) shows the experimental verification of quantized conductance in 2DEG [4]. This quantization is due to the presence of discrete channels for the transport of electrons and is a result of the nanoscale geometry.

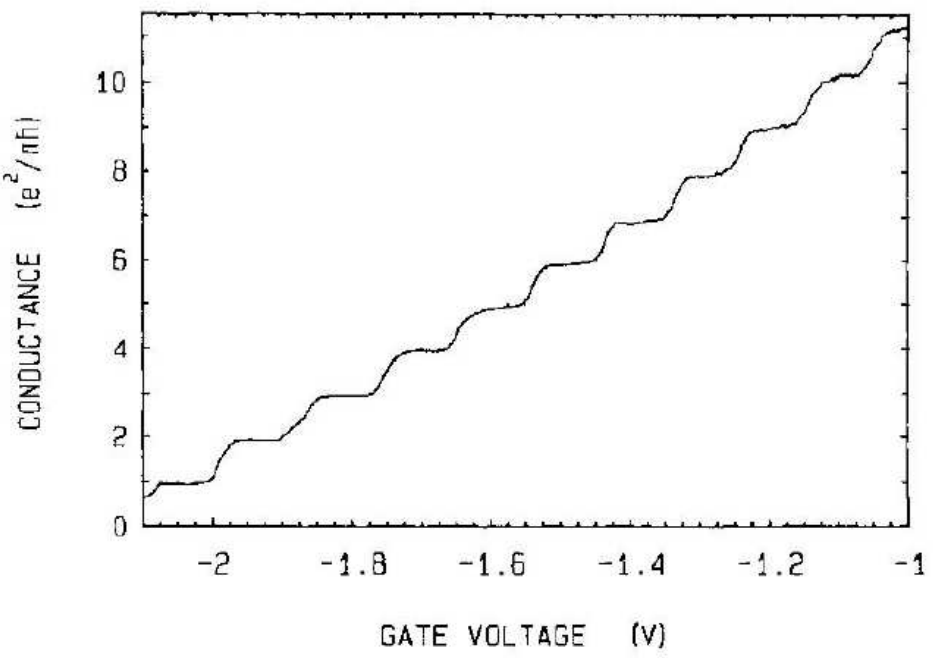

Figure 1.3: Quantization of conductance. This figure has been taken from [4].

Another important issue in mesoscopic transport is the consequence of high electron current density in nanoscale junctions. If a typical current of 1 μA is set to flow across the system, then, considering a cross-section of 10 Å^2, a current density of about 10^9 A/cm^2 is expected! These current densities are typically orders of magnitude larger than those found in macroscopic systems. The important consequence of this large current density is the phenomena of electron heating [9, 46]. Thus local electron or ionic heating in nanojunctions is also an important aspect in nanoscale transport that needs to be addressed by taking care of electron-electron and electron-phonon scattering. In this context I would again mention that subsequent chapters in this dissertation is motivated by these interesting phenomena that occur in such systems [10, 11, 54].

1.2 Overview of the thesis

The central topic of this thesis is an extensive study of transport in nanoscale systems. This dissertation is hence primarily devoted to understand the underlying formalisms that can be used to describe transport in low dimensional systems.

***Chapter* 2** is mainly an in-depth study of the Landauer-Büttiker formalism. A framework to connect the concepts of conductance, current and transmission in nanoscale systems is set up first. Subsequently, we focus on the transport properties of devices having transmission functions that depend on energy. The Sommerfeld expansion is used to obtain closed form expressions. We supplement the analytical results with numerical results. This chapter thereby provides a parameter regime in which the analytical expressions, obtained using this approximation, will work. In this chapter, I also try to address the question of asymmetric temperature in the leads that might arise in two situations, namely (a) when an explicit temperature difference is applied, or, (b) when the junction region might get heated up. Additionally, due to increasing attention towards the understanding of intrinsic noise in mesoscopic conductors, we also discuss about the importance and subtleties involved in the calculation of current noise power, again in the presence of a non-zero temperature gradient. We observe nonlinearity and asymmetry in current and noise power through these calculations. Our calculations also provide an insight into the form of the energy dependent transmission function. Analytical expressions of current noise power in the linear response regime, obtained in this chapter can help experimentalists, extract non-zero temperature differences in the leads. In the later part of the chapter, we discuss about the drawbacks of the Landauer-Büttiker formalism; one of the prime drawbacks being treating the impurity scatterer as a black-box.

***Chapter* 3** attempts to open the black-box in Chapter 2. In this chapter, I explicitly try to calculate the transmission function within the scattering region, using a model Hamiltonian. In a broader sense, this chapter may serve as a first step towards trying to explore the effect of the impurity scatterers present at the nanojunctions. The energy dependence of the transmission function may be obtained explicitly with the scheme used in this chapter. This calculation, however, is at its minimal level, in the sense that it is done for a 1-D chain of atoms with a very few number of atoms in the scattering region. The results obtained in this chapter depict important features that can develop in the transmission function if our system consists of onsite impurities. These features are important because Chapter 1 tells us that non-trivial energy dependence of the transmission function can give rise to asymmetric features in current across these systems in combination with the asymmetry induced by a finite temperature difference. Our goal is to try and implement this method for other kind of quantum systems like quantum point contacts or nanotubes.

***Chapter* 4** is more like a literature survey or a case study trying to relate the questions addressed in this thesis, to the ongoing study of *'Joule heating in nanoscale junctions'*.

Chapter 2

Landauer Approach

This chapter focuses on the understanding of transport in mesoscopic and nanoscale systems within the Landauer-Büttiker approach [13, 14].

This chapter is divided into the following sections:

Section 1: Formalism

- Introduction
- Foundations of the Landauer Approach
- Derivation of the equations for current and noise using the scattering matrix approach.

Following this would be a simple yet non-trivial application of the above approach to derive certain analytical expressions for charge current and charge current fluctuations. It is worth mentioning at this point that analyses motivated on similar

grounds have been reported more than once in different forms [15, 16, 24], for the energy current and energy current fluctuations. Being independently motivated, we focused on charge current and its fluctuations only to predict some interesting features in the quantities that are experimentally determined quite regularly in this field. So the later part of this chapter would consist of the following:

Section 2: Application to our problem

- Setting up the problem
- Discussion of the results
- Applicability of the results

Finally, I would like to conclude the chapter by a brief discussion about the drawbacks of the Landauer approach. So, the last part would consist of:

Section 3: Conclusion

- Drawbacks of the Landauer approach

Section 4: Summary and open questions

2.1 Formalism

2.1.1 Introduction

The Landauer [20] approach treats a non-equilibrium transport problem in the steady state as a scattering problem. It is based on certain physical assumptions

that will be discussed soon. It is to be noted that the physical assumptions on which the present approach is rooted may not be realized in all kinds of physical or experimental realizations, some of which shall be discussed towards the end of the chapter.

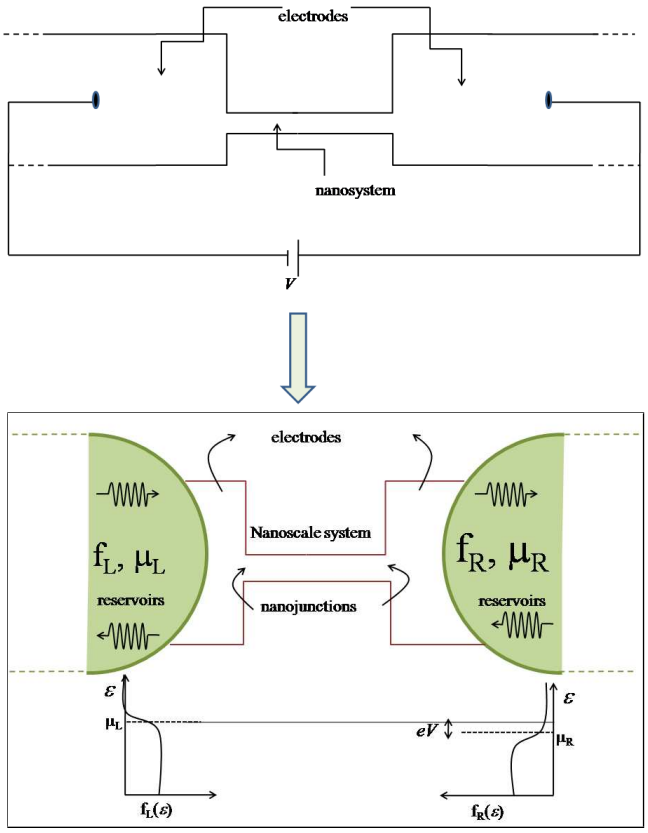

Figure 2.1: Mapping a closed quantum system onto an open quantum system via the introduction of reservoir of electrons

2.1.2 Foundations

We discuss the underlying assumptions of the Landauer-Büttiker formalism below:

[a] ***Visualizing a non-equilibrium closed system as an open quantum***

system in steady state

Before I proceed with the explanation of the above statement, let me describe the structure of our system . Our system consists of a region which is the device region through which we pass current by attaching a voltage source or a current source via electrodes. Physically, an experimentalist would like to probe the electron flow across the electrode-conductor-electrode system which is actually a closed system. But theoreticians find it easier to describe the battery or the electrodes as reservoirs of electrons. So the system is now mapped onto a region sandwiched between two large chunks of material that act as the environment. So the device now becomes open to two reservoirs with incoming electrons and outgoing electrons not talking to each other. This mapping is shown in figure (2.1).

Summary:

- **System is open to reservoirs which act as source and sink for electrons.**
- **For the reservoirs to behave as source or sink demands a difference in their chemical potentials and this difference is equal to the applied voltage gradient required to make the electrons flow.**

$$eV = \mu_L - \mu_R$$

- **The problem then is to try and understand how such a system interacting with two reservoirs would evolve dynamically.**

[b] ***Existence of a steady state***

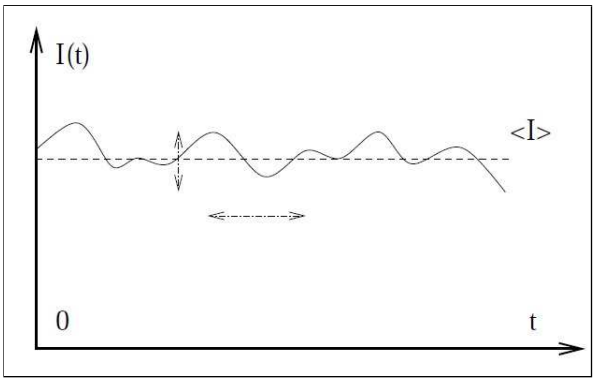

Figure 2.2: Fluctuations in average current

The Landauer approach presumes the existence of a steady state. Any analytic expression derived within this approach is only valid once the steady state has reached. By this statement we claim that if we wait long enough we will definitely reach a steady state when the density matrix of the system becomes time independent and one obtains a dc value for current at every instant of time, although there may be fluctuations about this dc value, like that shown in figure (2.2).

[c] ***Scattering takes place only at the junction***

In figure (2.1), which describes our system, the region where the device makes contact with the electrodes or the leads will be termed as 'nanojunction'. The Landauer approach assumes that scattering takes place only at the junction and otherwise the flow is ballistic [14].

- **The unique feature of the dimensions of the junction manifests itself in the scattering at the junction.**
- **This phenomenon cannot be neglected unlike bulk junctions. This form of scattering will always be present even if electron-phonon or electron-electron scattering is absent.**

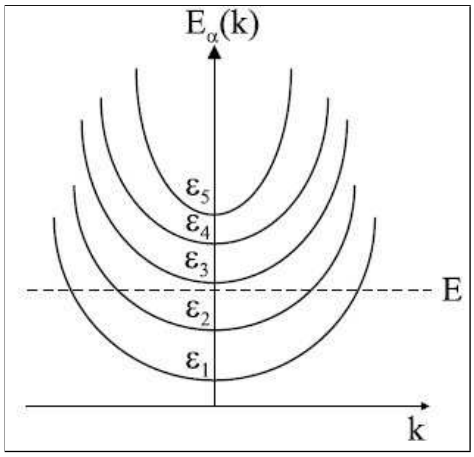

Figure 2.3: Presence of several discrete transverse channels for a continuum of longitudinal modes

[d] ***Use of appropriate boundary conditions to map the open quantum system to a closed one***

With the foundation underlined in [b] we can realize that the role of the reservoirs is to prepare the state of the electrons in the distant past or in the distant future. Also, the electrons in the reservoirs are assumed to be free and so we have the following asymptotic conditions:

$$\lim_{x\to-\infty} H_S = H_L = -\frac{\hbar^2}{2m}\nabla^2 + V_L(r_\perp); \quad S : \text{System}; \quad L : \text{Left},$$
$$\lim_{x\to\infty} H_S = H_R = -\frac{\hbar^2}{2m}\nabla^2 + V_R(r_\perp); \quad R : \text{Right}.$$

where, $H_{L(R)}$ is the Hamiltonian of the left(right) lead and $V_{L(R)}$ is the confinement potential in the same. The electrons are free in the x-direction and have extended states but do experience a transverse confinement. So, the energy eigenvalues consist

of a longitudinal part and a transverse part independent of each other,

$$E_n(k) = \epsilon_n + \frac{\hbar^2 k^2}{2m}, \tag{2.1}$$

and the wave functions are given by a product of the transverse and longitudinal parts,

$$\psi_{nk}(\vec{r}) = \sqrt{\frac{1}{L_x}}\ \chi_n(\vec{r_\perp})e^{ikx} \tag{2.2}$$

n: Different modes corresponding to the quantized states obtained by solving the Schrödinger equation in the transverse direction.

k: Motion along x-direction is obtained by solving a free electron Schrödinger equation and so it represents a free electron state.

- **Several transverse modes or channels of energy ϵ_n with discrete energies exist for a given continuum of longitudinal modes. These transverse modes are called channels [19, 26].**

- **The number of channels $N_c(E)$ for a particular energy is fixed so that,**

$$E_n(k) - \epsilon_n = \frac{\hbar^2 k^2}{2m} \quad > \quad 0$$

so,

$$N_c(E_n(k)) = \sum_n \Theta(E_n(k) - \epsilon_n)$$

[e] ***Channels are independent of each other***

The final approximation is that the channels do not interact with each other. The state of an electron moving through one channel is orthogonal to the state described by another channel.

2.1.3 Derivations of the equations for current and noise power within the Landauer formalism: The Scattering matrix Approach

The beauty of the Landauer approach lies in the possibility of mapping the entire problem of quantum transport in mesoscopic conductors to a simple scattering problem. It was first introduced by Landauer and further developed by Imry and Büttiker [14, 17, 25]. In the subsequent parts I will formulate the scattering problem and derive the famous Landauer formulae. We follow the notations in reference to [14, 26] in the following.

2.1.3.1 Scattering states

We visualize our system, (figure (2.4)) as a scattering system where the junctions behave as scatterers and the central device region is ballistic. This means the electron's state does not change until it encounters the other junction. So the central region is replaced by a *black box* and the junctions by a scatterer that changes the state of the incoming electrons. All of these features are put together in the figure (2.4).

Let us consider for simplicity that the electrons do not interact with each other. There are no inelastic processes taking place in the leads. The only equilibration

happening is in the reservoirs. Under such a situation, the electronic wave functions and energies can be written as equations (2.1) and (2.2).

At this point I would switch to the second quantized notation, wherein I will define field operators in terms of creation and annihilation operators in the respective leads. So I define the field operators,

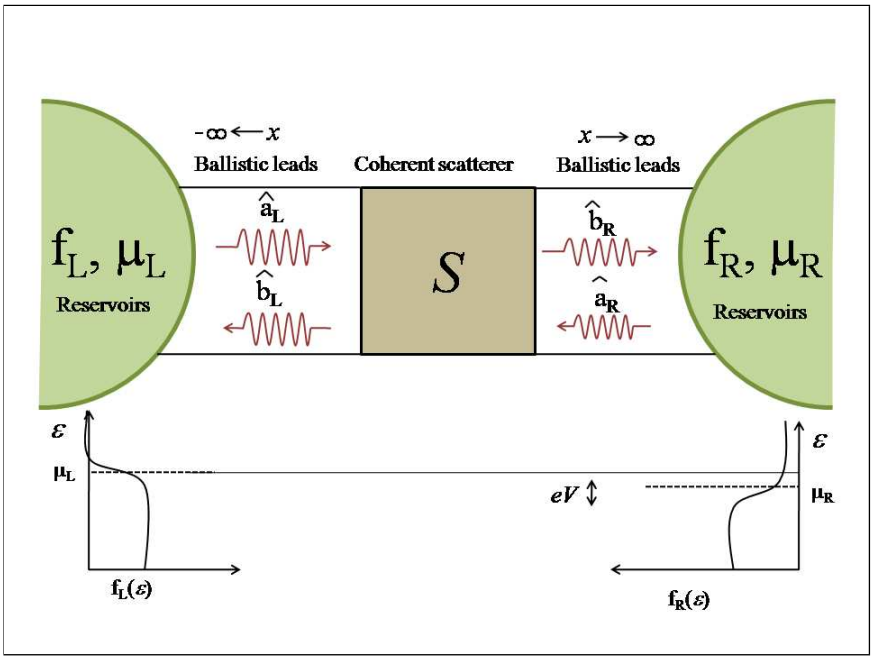

Figure 2.4: Schematic of the system as a scatterer with the ballistic leads consisting of incoming and outgoing scattered states

$\hat{\psi}_{L(R)}(\vec{r})$: Annihilates an electron in the (L) left ((R) right) lead at position $\vec{r}$.

$\hat{\psi}^{\dagger}_{L(R)}(\vec{r})$: Creates an electron in the (L) left ((R) right) lead at position $\vec{r}$.

$\hat{a}_{L(R)n,k}$: Annihilates an electron in the incoming state corresponding to channel n with wave-vector k, in the left(right) lead.

$\hat{b}_{L(R)n,k}$: Annihilates an electron in the outgoing state corresponding to channel n with wave-vector k, in the left(right) lead.

$\hat{a}^{\dagger}_{L(R)n,k}$: Creates an electron in the incoming state with the respective characteristics.

$\hat{b}^{\dagger}_{L(R)n,k}$: Creates an electron in the outgoing state with the respective characteristics.

So,

$$\hat{\psi}_L(\vec{r},t) = \frac{1}{\sqrt{L_x}} \int \mathrm{d}\epsilon \;\; e^{-i\epsilon t/\hbar} \;\; \sum_{n=1}^{N_L} \left(\hat{a}_{Ln}(k) e^{ikx} + \hat{b}_{Ln}(k) e^{-ikx} \right) \;\; \frac{\chi_{Ln}(\vec{r_\perp}) \;\; L_x}{2\pi\hbar \;\; v_{Ln}(\epsilon)}$$

$$\hat{\psi}^{\dagger}_L(\vec{r},t) = \frac{1}{\sqrt{L_x}} \int \mathrm{d}\epsilon \;\; e^{i\epsilon t/\hbar} \;\; \sum_{n=1}^{N_L} \left(\hat{a}^{\dagger}_{Ln}(k) e^{-ikx} + \hat{b}^{\dagger}_{Ln}(k) e^{ikx} \right) \;\; \frac{\chi^{*}_{Ln}(\vec{r_\perp}) \;\; L_x}{2\pi\hbar \;\; v_{Ln}(\epsilon)}$$

A more elaborate discussion is provided in Appendix A.

2.1.3.2 Scattering Matrix

Now that we have formulated our problem as a scattering problem that can be defined in terms of incoming and outgoing scattering state operators, we move on to defining the relation between them. The outgoing state operators and the incoming

state operators are related via the scattering matrix, S, as follows,

$$\hat{b} = S\hat{a} \tag{2.3}$$

For an M terminal device,

$$S = \begin{pmatrix} S_{11} & S_{12} & \dots & S_{1M} \\ S_{21} & S_{22} & \dots & S_{2M} \\ \dots & \dots & \dots & \dots \\ \vdots & \vdots & \vdots & \vdots \\ S_{M1} & S_{M2} & \dots & S_{MM} \end{pmatrix}$$

where, each of these blocks $S_{\alpha\beta}$ is a matrix of dimension (N_α x N_β); N_α being the number of channels in the αth lead.

Hence,

$$\hat{b}_{\alpha n}(\epsilon) = \sum_{\gamma} \sum_{k=1}^{N_\gamma} S_{\alpha n,\gamma k} \hat{a}_{\gamma k}(\epsilon)$$

More compactly,

$$\hat{b}^\dagger_{\alpha n}(\epsilon) = \sum_{\gamma} \sum_{k=1}^{N_\gamma} \hat{a}^\dagger_{\gamma k}(\epsilon) \left(S^\dagger_{\alpha\gamma}\right)_{kn} \tag{2.4}$$

$$\hat{b}_{\alpha n}(\epsilon) = \sum_{\gamma} \sum_{k=1}^{N_\gamma} \left(S_{\alpha\gamma}\right)_{nk} \hat{a}_{\gamma k}(\epsilon) \tag{2.5}$$

with,

$(S_{\alpha\alpha})_{ij} = r_{ij}$	Responsible for **reflection** of a carrier in the incoming state in lead 1 channel i, to an outgoing state in lead 2, channel j.
$(S_{\alpha\beta})_{ij} = t_{ij}$	Responsible for **transmission** of a carrier in the incoming state in lead 1, channel i, to an outgoing state in lead 2, channel j.
$(S_{\beta\alpha})_{ij} = t'_{ij}$	Responsible for **transmission** of a carrier in the incoming state in lead 2, channel i, to an outgoing state in lead 1, channel j.
$(S_{\beta\beta})_{ij} = r'_{ij}$	Responsible for **reflection** of a carrier in the incoming state in lead 2, channel i, to an outgoing state in lead 2, channel j.

[a] Average Current

The current operator for lead α is given as the probability current operator (times the charge carrier), in terms of the field operators,

$$\hat{I}_\alpha(x,t) = \frac{\hbar e}{2im}\int \mathrm{d}\vec{r}_\perp \left[\hat{\psi}^\dagger_\alpha(\vec{r},t)\frac{\partial}{\partial x}\hat{\psi}_\alpha(\vec{r},t)\right] - \left(\frac{\partial}{\partial x}\hat{\psi}^\dagger_\alpha(\vec{r},t)\right)\hat{\psi}_\alpha(\vec{r},t)$$

We can now substitute the explicit forms of the incoming and outgoing state operators. Based on the following assumptions, we converge to a closed expression for the current in the lead α. The assumptions are :

1. For all observable quantities, ϵ and ϵ' either coincide or are close to each other. This means that the eigen spectrum is very closely spaced for the energies relevant to transport, i.e. in a window around the Fermi energy, ϵ_F.

2. The velocities are almost constant and scale with the Fermi velocity.

In this limit, we get,

$$\hat{I}_\alpha(t) = \frac{e}{2\pi\hbar}\sum_n \int\int \mathrm{d}\epsilon \;\; \mathrm{d}\epsilon' \;\; e^{i(\epsilon-\epsilon')t/\hbar}\left[\hat{a}^\dagger_{\alpha n}(\epsilon)\hat{a}_{\alpha n}(\epsilon') - \hat{b}^\dagger_{\alpha n}(\epsilon)\hat{b}_{\alpha n}(\epsilon')\right]. \tag{2.6}$$

Equation (2.6) is general for any M terminal device. Here we consider a two terminal device for our further calculations[1]. Substituting for the outgoing state operators in the above equation we get, for a two terminal device[2],

$$\boxed{\left\langle \hat{I}_\alpha \right\rangle = \frac{e}{2\pi\hbar}\int_0^\infty \mathrm{d}\epsilon \;\; \sum_n T_n(\epsilon) \;\; \left[f_\alpha(\epsilon) - f_\beta(\epsilon)\right]} \tag{2.7}$$

where,

$T_n(\epsilon)$ are the eigenvalues of the matrix $t^\dagger t$,

and, f_α, f_β are the Fermi distribution functions with $\mu_\alpha - \mu_\beta = eV$. From the above equation we can readily realize that flux conservation demands,

$$\mathrm{Tr}(tt^\dagger) = \mathrm{Tr}(t't'^\dagger)$$

[b] Current Noise Power

In this part we proceed to understand another experimentally observed quantity namely the power spectrum of the current noise which is just the fourier transform of the autocorrelation function of the temporal fluctuations in current.

[1]The details can be obtained from Appendix A.
[2]$\alpha, \beta \equiv L, R$, respectively, globally

Unlike average current, the current-current correlation function or equivalently the fluctuations are more sensitive to the microscopic details of the system. Hence, the effects that are washed out in the case of average current are not necessarily suppressed in the case of fluctuations. Thereby, they serve as a probe to the microscopic phenomena occurring in our system.

Current noise can be *intrinsic* or *extrinsic* in nature. Among *extrinsic* sources we have the $1/f$ noise [27] which can be reduced by tuning the external conditions such as pressure or synthesis. The *intrinsic* noise is inherent to the system and is present even if the sample is completely pure. It cannot be avoided. There are two types of intrinsic noise, namely, *thermal* and *shot* noise.

[i] Thermal Noise

This type of noise arises because of the random fluctuations in the electron distribution at a finite temperature through the coupling to the reservoir. It provides information about the conductance of the system. Since these fluctuations are present in equilibrium conditions as well, the thermal noise power may be obtained directly from the *fluctuation-dissipation* theorem. It is also called the *Johnson-Nyquist* noise [21, 22].

[ii] Shot Noise

Shot noise on the other hand is a non-equilibrium phenomenon and arises due to quantization of charge in the case of electrons or energy in the case of photons. The shot noise in electrical current thus reflects on the randomness associated with the transmission of discrete charge quanta across the conductor.

Noise in nanoscale conductors

Noise becomes more perceptible and significant in nanoscale dimensions. To explain why it is so, I would like to cite the following example, in reference to figure (2.5):

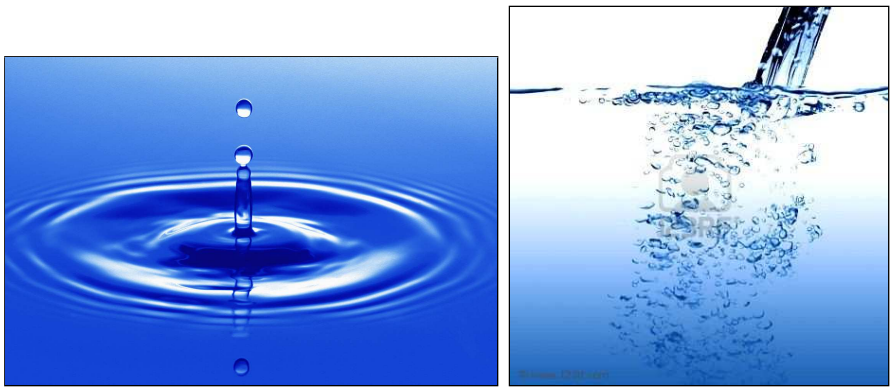

Figure 2.5: The figure on the left shows the arrival of water as droplets unlike the figure on the right which represents bulk flow or an average flow. *Courtesy*: Google Images

Imagine hearing the droplets of water fall. When the flow of water is not very large, the arrival of water droplets as discrete quanta is still realizable. However, we fail to recognize the discreteness when the water flow starts becoming very large. This is the same situation as in bulk conductors where the granularity of charge is lost and one is only able to perceive an average current. In other words, the fluctuations that are of the order of $1/\sqrt{N}$ and are small for N in the thermodynamic limit would be much larger for nano objects simply because of the smaller N.

Mathematical Details

The noise power corresponding to leads $\alpha, \beta(L, R)$ in Fourier space is given by,

$$P_{\alpha\beta}(\omega) = 2\int_{-\infty}^{\infty}\Big[\langle I_\alpha(t)I_\beta(t')\rangle - \langle I_\alpha(t)\rangle\langle I_\beta(t')\rangle\Big]e^{i\omega(t-t')}\mathrm{d}(t-t')$$

For static bias and in steady state,

$$\tilde{P}_{\alpha\beta}(t,t') = \tilde{P}_{\alpha\beta}(t-t')$$

Use of the scattering matrix formalism along with the properties of the scattering matrix yields the following in the static limit [14, 23, 18],

$$\begin{aligned}P_{\alpha\beta}(\omega=0) =(-1)^\zeta\int_0^\infty\Big(&\mathrm{Tr}\left\{\left(tt^\dagger\right)^2\right\}f_\beta\left(1-f_\beta\right)+\mathrm{Tr}\left\{\left(t't'^\dagger\right)^2\right\}f_\alpha\left(1-f_\alpha\right)\\&+\mathrm{Tr}\left\{tt^\dagger\left(\mathbb{1}_\alpha-tt^\dagger\right)\right\}\left[f_\alpha+f_\beta-2f_\alpha f_\beta\right]\Big)\mathrm{d}\epsilon\end{aligned}\tag{2.8}$$

where,

$$\zeta = \delta_{\alpha\beta}+1$$

The details can be obtained from the derivation given in Appendix C. We note that the transmission function would in general be a function of energy.

Equilibrium Noise

This would be defined as the noise with zero thermal and voltage bias i.e.,

$$
\begin{aligned}
& V = 0 \quad \text{and} \quad T_L = T_R = T, \\
& f_\alpha = f_\beta, \\
& \therefore \quad P_{\alpha\beta}(0) = 4k_B T \frac{e^2}{h} \mathrm{Tr}\left\{tt^\dagger\right\} \\
& \text{or} \;\; P_{\alpha\beta}(0) = 4k_B T \frac{e^2}{h} \sum_n T_n(\epsilon)
\end{aligned}
$$

$$
P_{\alpha\beta}(0) = 4k_B T G \;\; : \text{Fluctuation} - \text{Dissipation} \;\; \text{theorem[21, 22]}
$$

Here lies the origin of conductance quantization as observed in several nano devices [4] and illustrated in figure (1.3). By tuning an external parameter, if one can access a varying number of perfectly transmitting channels, then one would see the conductance developing plateaus.

Shot Noise as mentioned before is a purely non-equilibrium phenomenon and at zero temperature can be derived easily.

$$
\begin{aligned}
& T = 0 \\
& f_\alpha(1 - f_\alpha) = f_\beta(1 - f_\beta) = 0 \\
& \mu_\alpha - \mu_\beta = eV
\end{aligned}
$$

thus,

$$P_{\alpha\beta}(0) = \frac{2e^2}{h}\left(\sum_n T_n(1-T_n)\right)eV$$

So the shot noise power at $T = 0$ K, is just proportional to the applied voltage bias, V.

2.2 Application of the Landauer-Büttiker formalism to our problem

2.2.1 Setting up the problem

We try to visualize a situation in which the nano device is subjected to an asymmetry. Let us imagine a scenario where both voltage and temperature gradients are present across the electrodes. Such a situation is very likely to arise at least in two cases (i) the two electrodes heat up to different extents due to current flow (Joule heating), (ii) an explicit thermal gradient is applied. But it is to be noted that we also assume, for our present calculations that the interactions (e-ph scattering, e-e scattering, etc.) that drive this kind of heating are fast enough to equilibrate the electron to the temperature of the leads.

We also assume that the temperature gradient created in the leads extend across the lead in the true thermodynamic sense, so that equilibrium thermodynamic distribution functions can be defined with respect to it. I tried to justify our motivation in doing the above, in Chapter 4, wherein I have given recent examples that validates

our assumption.

2.2.2 Results

In this part I will present the features that we got because of the asymmetric situation discussed above. First I will discuss about current and then give the results on noise analysis.

In order to utilize the asymmetric situation (namely the presence of thermal bias) we have applied a time varying symmetric potential (square wave potential). The time period of the signal is much greater than the time scales in the system and hence a steady state analysis is always valid. It turns out that even for such a simplified situation we observe some non-trivial features which I will summarize, after each of the relevant figures.

2.2.2.1 Current

The steady state current in one of the leads (say, the left (L) lead) is given by,[3]

$$I_L(V) = \frac{e}{h}\int_0^\infty t(\epsilon)(f_L - f_R)\mathrm{d}\epsilon \ .$$

By usual notation, $\beta_{1(2)} = \frac{1}{k_B T_{1(2)}}$, where, T_1 is the temperature of lead $1(L)$ and T_2 is the temperature of lead $2(R)$; $T_1 \neq T_2$ and $T_1 - T_2 = \Theta$. I call this situation to be asymmetric because, when,

[3]From now onwards I will denote transmission probability as $t(\epsilon)$ and not $T(\epsilon)$ to distinguish it from temperature

- $V > 0, \mu_1 > \mu_2$,

$$\begin{aligned} I_L(V) =& \frac{e}{h}\int_0^\infty t(\epsilon)\ \mathrm{d}\epsilon \left[\frac{1}{1+e^{\beta_1(\epsilon-\mu_1)}} - \frac{1}{1+e^{\beta_2(\epsilon-\mu_2)}}\right] \\ =& \frac{e}{2h}\int_0^\infty t(\epsilon)\ \mathrm{d}\epsilon\ \frac{\sinh\left\{(\beta_2-\beta_1)\frac{\bar{\epsilon}}{2} + \beta_1\frac{eV}{2}\right\}}{\cosh\left\{\frac{\beta_1}{2}(\bar{\epsilon}-eV)\right\}\cosh\left\{\frac{\beta_2}{2}\bar{\epsilon}\right\}}\ . \end{aligned} \tag{2.9}$$

- $V < 0, \mu_2 > \mu_1$ (Source and drain interchanged),

$$I_L(V) = \frac{e}{2h}\int_0^\infty t(\epsilon)\ \mathrm{d}\epsilon\ \frac{\sinh\left\{(\beta_2-\beta_1)\frac{\bar{\epsilon}}{2} - \beta_2\frac{e|V|}{2}\right\}}{\cosh\left\{\frac{\beta_1}{2}\bar{\epsilon}\right\}\cosh\left\{\frac{\beta_2}{2}(\bar{\epsilon}-e|V|)\right\}}\ . \tag{2.10}$$

The origin is chosen as the following:[4]

$V = 0 \longrightarrow \mu_1 = \mu_2 = \mu.$

$V > 0 \longrightarrow \mu_1 = \mu + eV,\ \epsilon_0 = \mu + x.$

$V < 0 \longrightarrow \mu_2 = \mu + eV,\ \epsilon_0 = \mu + x.$

and, $\bar{\epsilon} = \epsilon - \mu$.

So,

$I_L(V, T_1, T_2) \neq -I_L(-V, T_1, T_2)$.

If $\beta_1 = \beta_2$, we can easily see that, $I_L(V) = -I_L(-V)$.

[4]We have not considered any bias dependence in the transmission function.

I now take up specific forms of $t(\epsilon)$ to do further calculations.

- **Case 1 $\Rightarrow$ $t(\epsilon)$: flat function of energy**

In the limit ($k_BT << \mu_1(\mu_2)$), $I_L(V)$ is same as in the symmetric case.

- **Case 2 $\Rightarrow$ $t(\epsilon)$: Lorentzian**

$$t(\epsilon) = \frac{w\alpha}{\pi} \frac{1}{\{(\epsilon - \epsilon_0)^2 + w^2\}} \tag{2.11}$$

w : width of the Lorentzian;

ϵ_0 : centre of the Lorentzian (chosen to be around the equilibrium Fermi energy μ).

If $t(\epsilon)$ varies slowly around the chemical potential μ_1 and μ_2 then we can use the Sommerfeld expansion [28]; the steps are outlined in Appendix E. We then get,

$$I_L(+V) + I_L(-V) = \Delta I_L(V) = \frac{w\alpha\pi}{3} \; k_B^2 \; A(V) \left[T_1^2 - T_2^2\right] \frac{e}{h} \tag{2.12}$$

where, $A(V) = \frac{x}{(x^2+a^2)^2} - \frac{eV-x}{\{(eV-x)^2+a^2\}^2}$.

The above equation gives the directed current because of the presence of an asymmetric situation induced by a non zero temperature gradient.To check the validity of the Sommerfeld expansion we numerically integrated equations (2.9) and (2.10) with $t(\epsilon)$ as given by (2.11). Figure (2.6) shows the agreement of the analytical expression according to (2.12) and numerical integration of (2.9) and (2.10). A parameterization is shown in figure (2.8) where one can find out the temperature and voltages where the Sommerfeld expressions can be used.

The parameters used for figures (2.6 - 2.8) are given by $x = 0,\ w = 1$ eV$, \mu =$ 5 eV, $\Theta = 400$ K.

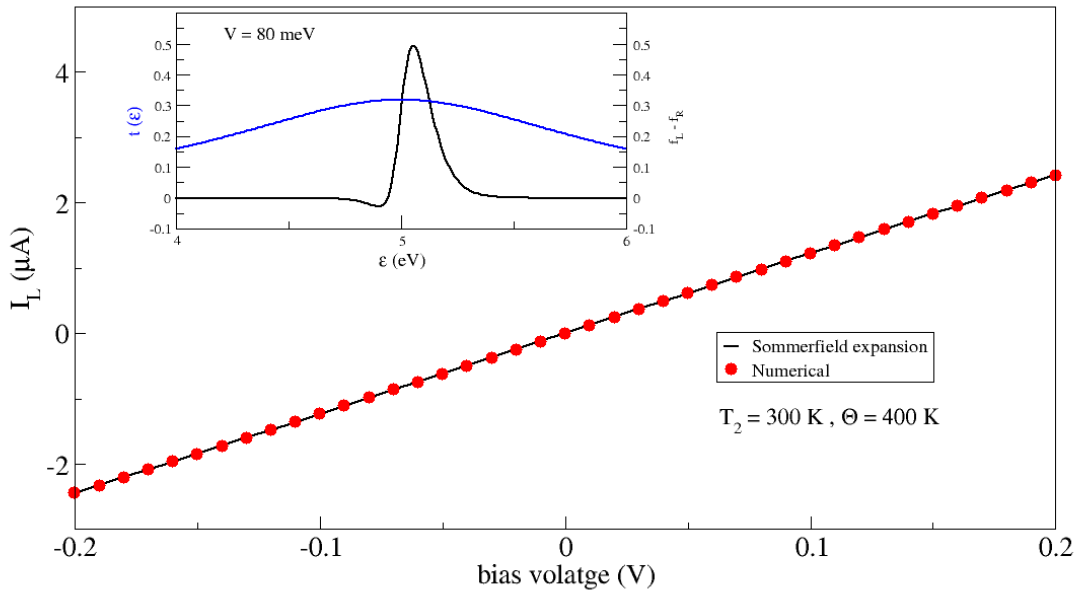

Figure 2.6: Current calculated using both Sommerfeld expansion (analytical solution) and numerical integration. The transmission function is shown in the inset as $t(\epsilon)$.

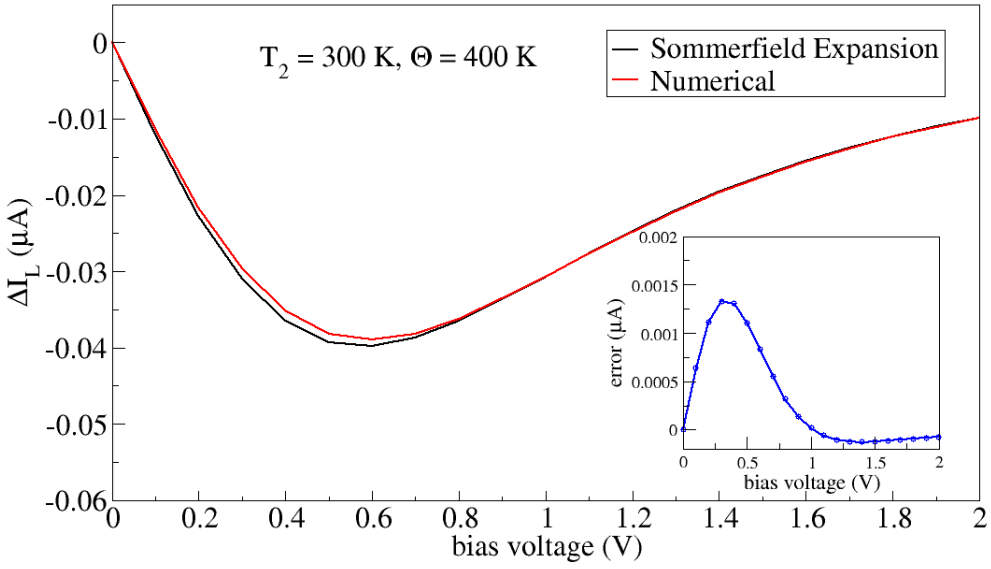

Figure 2.7: Net current calculated using both Sommerfeld expansion (analytical solution) and numerical integration.

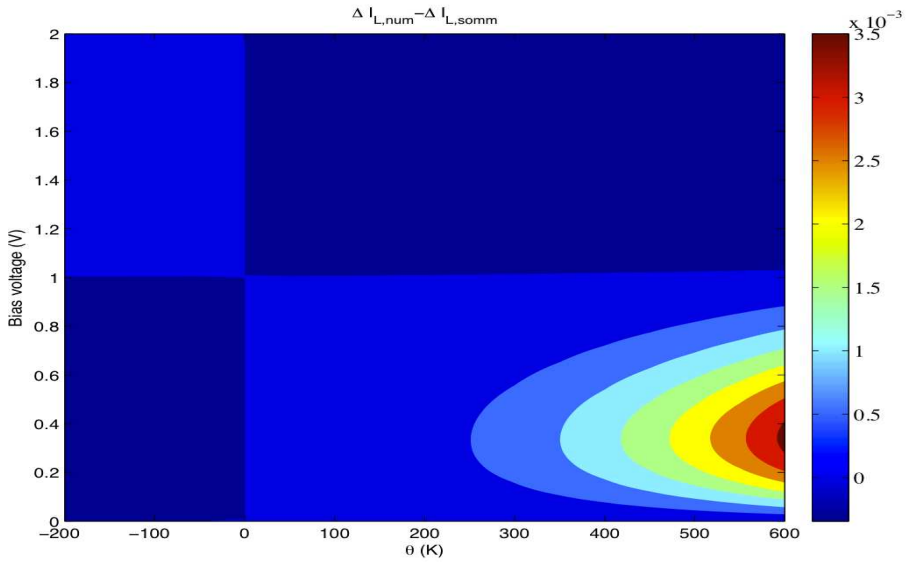

Figure 2.8: Parameter space in V and Θ where the Sommerfeld expansion is valid.

- **Case 3 $\Rightarrow$ $t(\epsilon)$: Sharp function of energy**

For this case we again consider a Lorentzian but the parameter $w \sim k_B T$.

- For such a situation we cannot use any approximation as can be seen from figure(2.9). So, we have to integrate (2.13) numerically.

- The net (directed) current is plotted in fig.(2.10) for three different peak positions of the transmission function. The parameters used are: $x = (0, 0.05, -0.05)$ eV $w = 50$ meV, $\mu = 5$ eV, $\Theta = 400$ K. It is observed that the net current possesses a flat minima that changes its position with a change in the position of the sharp maxima of the transmission function in the energy space. The direction of this shift is the same as the direction of the shift in the peak position.

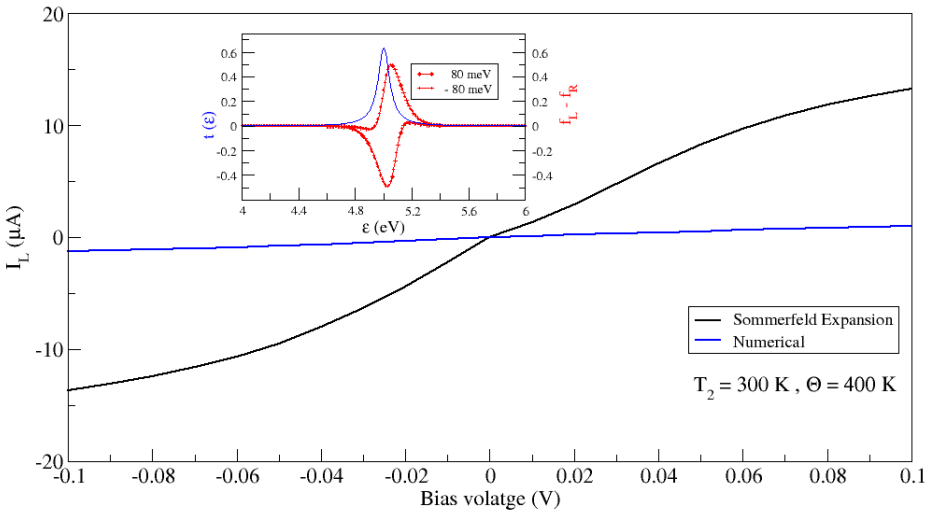

Figure 2.9: This figure plots current as a function of the applied bias and shows the invalidity of the Sommerfeld expansion for the transmission function shown in the inset. This is general for any transmission function with the $w \sim k_B T$.

- Another important feature is noticed in figure(2.11) where the net current is plotted as a function of applied voltage but for different Θ. There exists a universal voltage for a particular x (here $x = 0.05$eV) at which there is current reversal. This voltage is independent of the temperature gradient Θ.

2.2.2.2 Summary

- We observe a rectification of current on application of a slowly varying square wave potential. This is due to the presence of both voltage and temperature gradient. The sign of the current depends on the competition between both these effects to move the electron (figures (2.7 and 2.10)).

- The amount of rectified current is $\sim nA$ for relatively flatter functions (figure 2.7) and $\sim \mu A$ for very sharp transmission functions (figure 2.10).

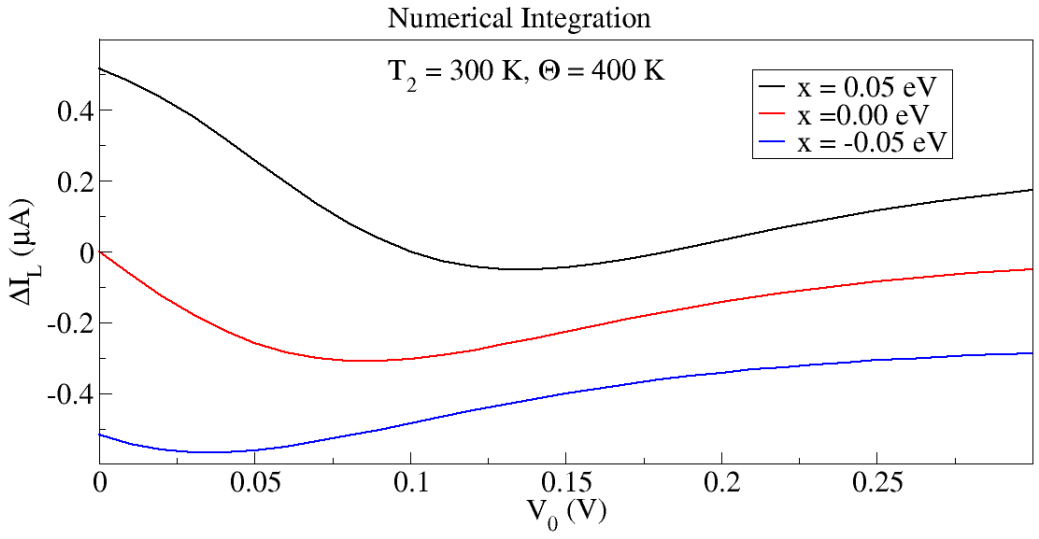

Figure 2.10: Net directional current is plotted as a function of the applied bias. V_0 is the amplitude of the applied square wave potential. In the equations V_0 is the same as V. The above is plotted for three different x's or peak positions of the transmission function shown in the inset of figure(2.9), (i) shifted slightly to the right of the chemical potential, (ii) at the chemical potential, (iii) shifted slightly to the right of the chemical potential.

- Thus the amount of the directional current can inform us about the qualitative features of the transmission funcion. However we have considered only one open channel for all our calculations.

- Also the value of the bias voltage at which a reversal of net current (change in sign) occurs varies with the peak position of the transmission function. So, that again informs us about the transmission function.This dependence of V on x is found out to be a straight line. This is shown in figure (2.12).

- We have done a parameterization for the directed current with V and x. A parameterization with other parameters of the transmission function is also necessary to get a better insight.

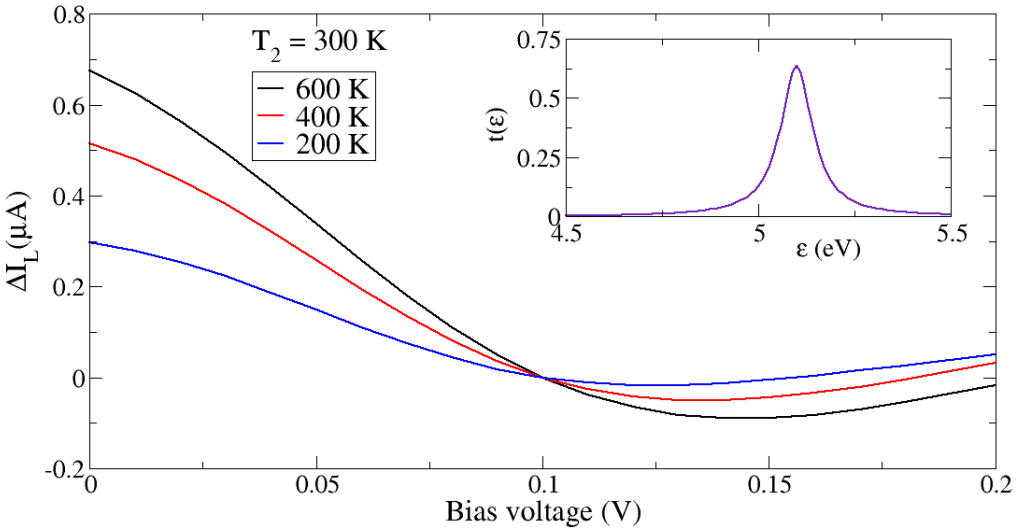

Figure 2.11: Net directional current is plotted as a function of the (amplitude of the) applied bias as in figure (2.10), but for different Θ. The above is plotted for a transmission function, (shown in the inset) that is slightly shifted to the right of the chemical potential.

- The following question needs to be addressed:

  Are there any special features in the noise power spectrum on changing the applied bias volatge and temperature gradient?

While the last point is addressed in the next section, the penultimate one could not be answered in this thesis. We are hopeful to come up with a more plausible explanation and analysis soon.

2.2.2.3 Current Noise

The current noise power is given by (2.8). When the transmission function is an approximately flat function of energy, one can solve (2.8) exactly to obtain the

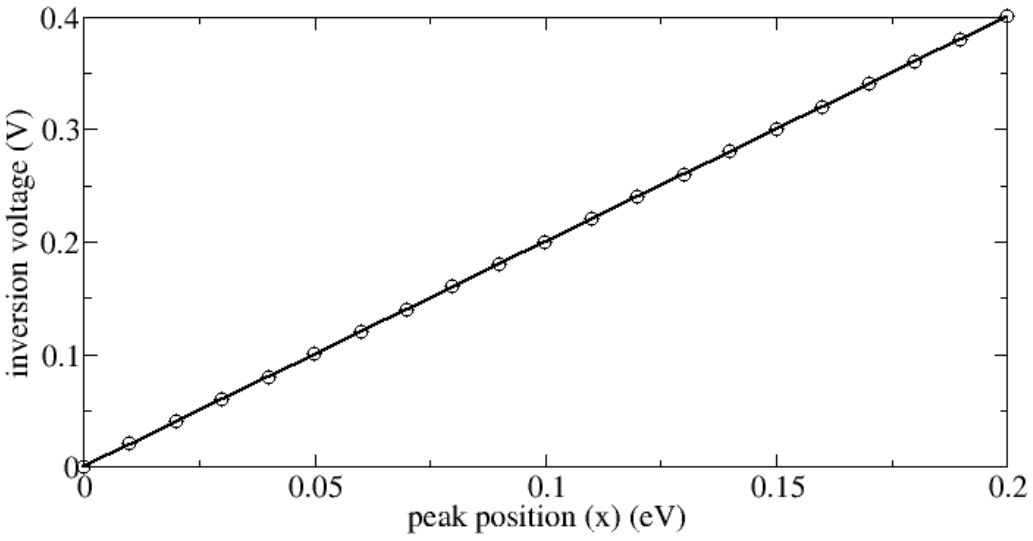

Figure 2.12: Voltage at which current reversal occurs is plotted as a function of the position of the peak of the transmission function (w.r.t the chemical potential. The above is plotted for values of x which are slightly shifted to the right of the chemical potential. of the chemical potential. It depicts a perfect straight line behaviour with slope =2.

following relation:

$$P(V,T) = \frac{2e^2}{h} \sum_n \left[2k_B T \;\; T_n^2 - T_n \Big(1 - T_n \Big) eV \coth \frac{eV}{2k_B T} \right], \tag{2.13}$$

where, I have removed the lead indices because by flux conservation and time reversal symmetry, $P_{\alpha\alpha} = P_{\beta\beta} = -P_{\alpha\beta} = -P_{\beta\alpha}$. Let α denote the left (L) lead and β denote the right (R) lead. The noise power is represented by the above equation when $T_1 = T_2$. But, similar to what has been done for current let us now consider the asymmetric situation of $T_1 \neq T_2$.

- **Case 1 $\Rightarrow$ $t(\epsilon)$: flat function of energy**

Using the steps detailed in Appendix D, we can arrive at the following closed form expression in this case[5]:

-

$$P(V,T,\Theta) = P_0(V,T,\Theta) + k_B \sum_n \Big(\Theta\ T_n^2 + \Theta\ T_n(1-T_n)\Big)\left(\frac{\bar{V}}{2\sinh(\bar{V}/2)}\right)^2, \tag{2.14}$$

where, $P_0(V,T,\Theta)$ is given by (2.13). Here we have considered the ambient temperature, T, to be that of the right lead. Looking at the above expression we can realize that it is an even function of V. Hence, interchange of the source and drain electrodes is not going to give us anything interesting, although we would see shortly that, this is not the case with an energy dependent transmission function.

- Figure(2.13) and figure(2.14) is a comparison between the analytical and the numerical result. The latter refers to the numerical integration of (2.8). Figure(2.13) is for a very low temperature difference ($\sim$ 50 K), while figure(2.14) is for a relatively high $\Theta \sim$ 400 K. As can be seen from figure(2.15), there is a linear increase in the error between the numerical and the analytical expression, with increase in the value of Θ. This is because we have limited our analysis to linear order in Θ, when we expanded f_L in a Taylor series. This can be clearly understood from Appendix D.

[5]The expressions are in units of $\frac{2e^2}{h}$

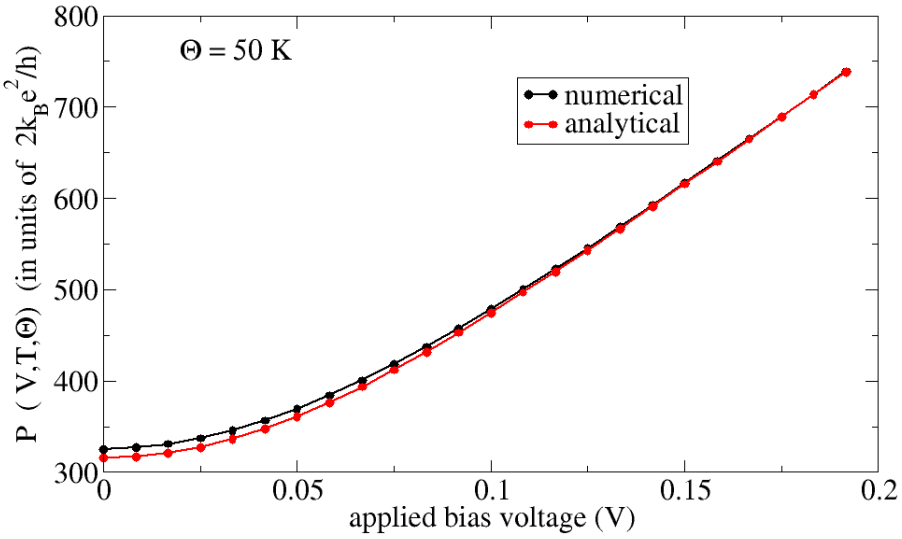

Figure 2.13: Current noise power in presence of a finite temperature difference ($\Theta = 50$ K) in the leads. It also shows a comparison between the numerical and analytical calculation ((2.15)). The error becomes less as one approaches higher voltages.

- The important thing to note is that the error is very small, especially for high bias (~ 0.1 V), low Θ, which means the analytical expression can be used in this regime with minimal error. This is shown in figure (2.15).

- Also, since the error is very small for low Θ, one can use it to predict the Θ using the expression for the linear response regime in voltage, namely[6],

$$\lim_{V\to 0} \Delta P = \sum_n T_n k_B \Theta. \tag{2.15}$$

As can be seen from figure(2.16), when Θ is 50 K, the enhancement in noise is ~ 25 K, while the enhancement predicted by (2.15) is also 25 K. So (2.15) can be used reliably to get an idea about low temperature changes in the leads, if

[6]The following expression is in unit of $\frac{2e^2}{h}$

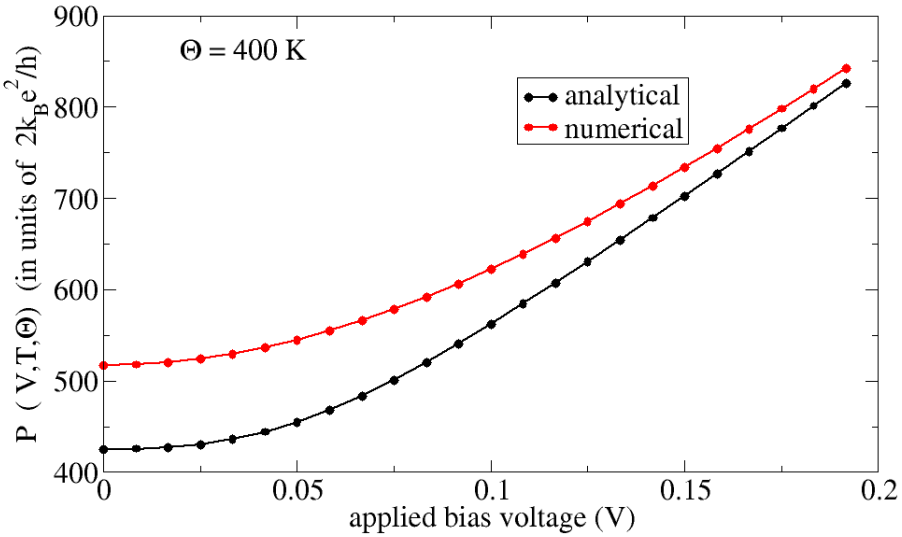

Figure 2.14: Current noise power in presence of a finite temperature difference ($\theta = 400$ K) in the leads. The error is much more than $\Theta = 50$ K, because of the consideration of linear order in Θ to do the calculation.

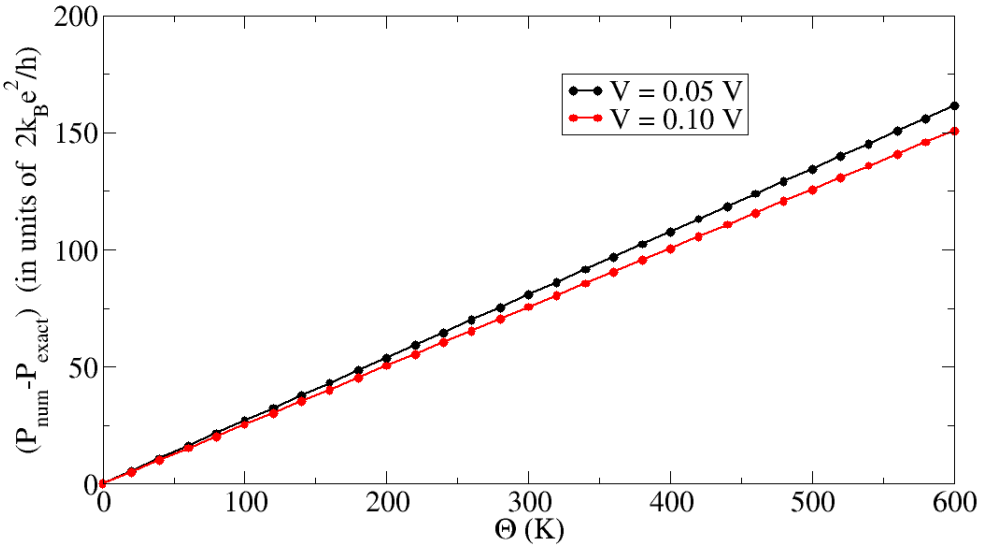

Figure 2.15: This figure shows a linear increase in the error with increase in the value of Θ. It is to be noted that the error decreases with increase in the bias.

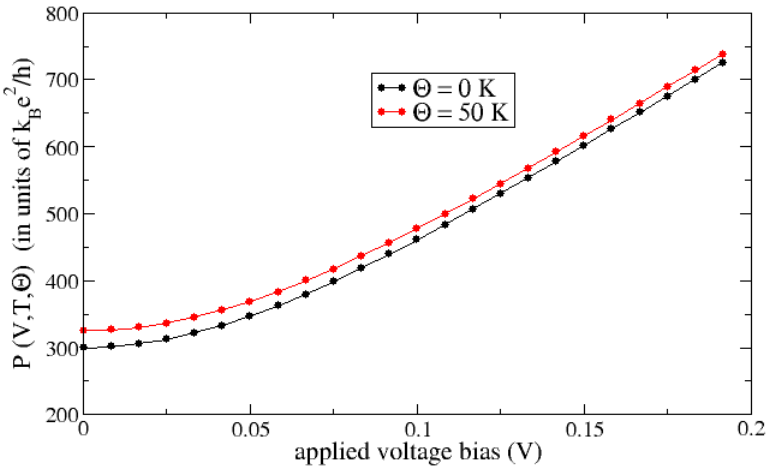

Figure 2.16: This figure shows the increase in noise due to a non-zero value of Θ. At $V = 0$, this increase is to be related to the thermal noise. This can therefore be used to extract the value of Θ.

any.

- **Case 2 $\Rightarrow$ $t(\epsilon)$: function of energy (Lorentzian)**

Now let us consider the transmission function to be dependent on energy in the form of a Lorentzian given by (2.11). Here, I present the numerical results wherein (2.8) is evaluated numerically. The parameters used for $t(\epsilon)$ is again the same as used for current; figures (2.17) and (2.18) are plotted using the parameter x in $t(\epsilon)$ as 0 eV.

- Figure (2.17) again shows the enhancement of noise power due to a nozero temperature difference in the leads. The other important thing to note is the change in the shape of the curve from the $\Theta = 0$ stuation. For $\Theta = 0$, the minima occurs at $V = 0$, but now this minima shifts towards higher applied bias voltages with increase in the value of Θ.

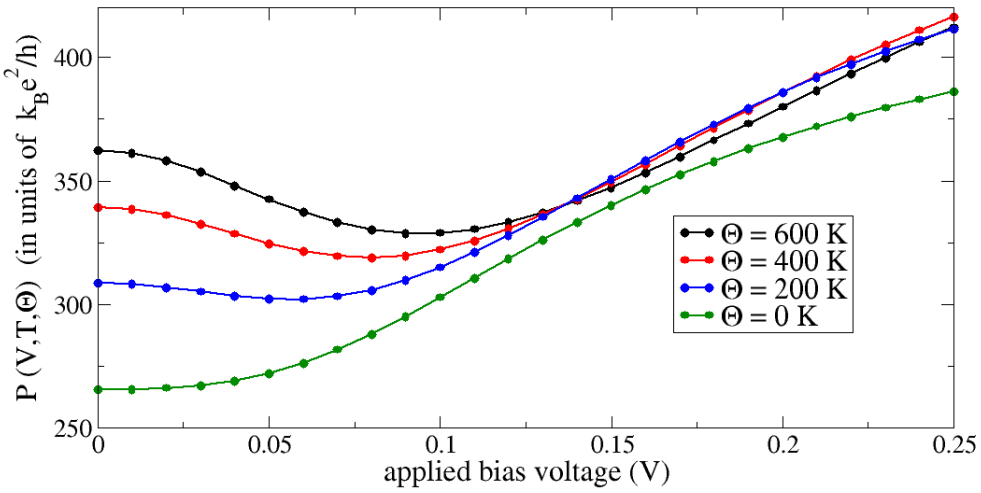

Figure 2.17: This figure plots the current noise power as a function of V for different Θ. Apart from an enhancement, now the minima shifts from $V = 0$, with increase in Θ.

- In figure (2.18) we plot the change in noise power due to change in voltage polarity. ΔP here is equal to $P(+V) - P(-V)$. Here, again, we notice a minima like the one observed for ΔI. This minima shifts towards higher V with increase in the value of Θ.

- Now we consider a different value of x(=0.05 eV). For ΔI we observed a universal crossing point at 0.1 V. Here also we notice the same crossing voltage, where ΔP changes sign. There is a crossing at 0 V also, but that is because at $V = 0$ it is only thermal noise in action. This observation is shown in figure (2.19).

- **Case 3 $\Rightarrow$ $t(\epsilon)$: Lorentzian (Analytical solution)**

The analytical solution could not be a part of this thesis, however, the scheme is outlined in Appendix E. We can again use the Sommerfeld expansion [28] to for

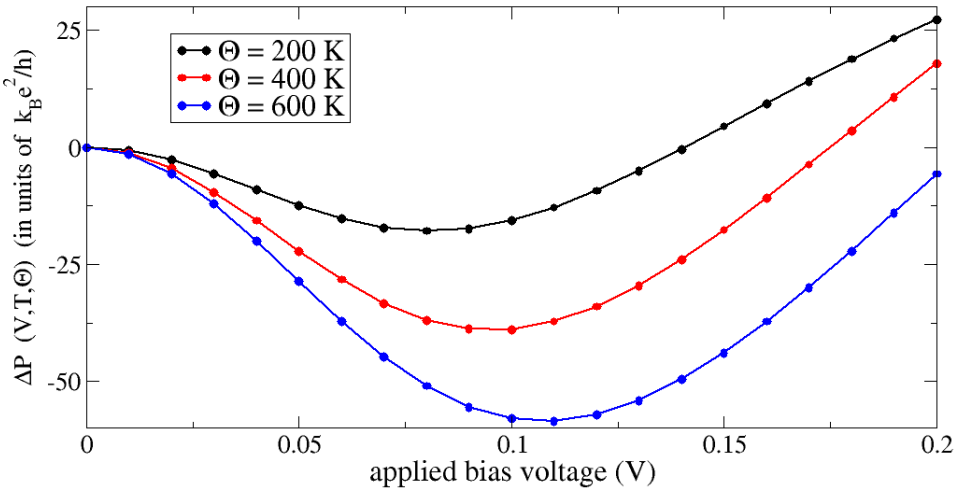

Figure 2.18: ΔP plotted as a function of V; $x = 0$ eV.

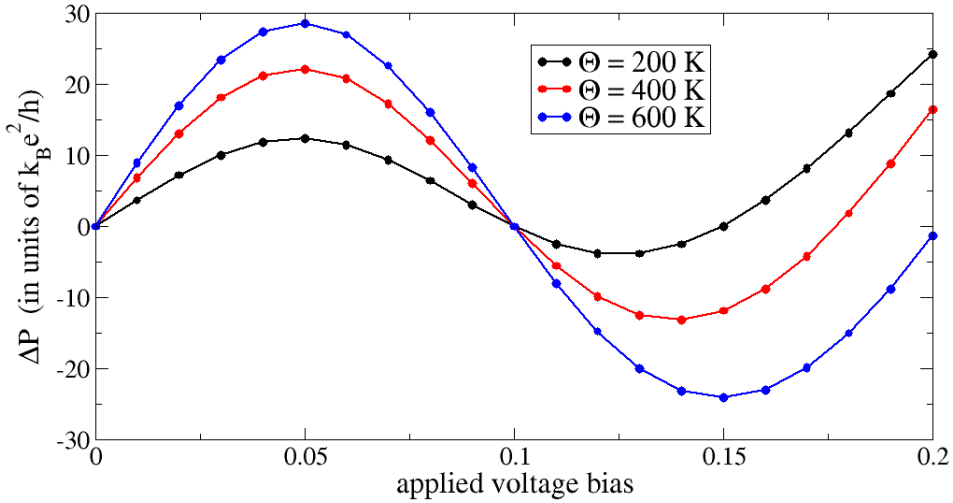

Figure 2.19: ΔP plotted as a function of V; $x = 0.05$ eV.

this case, keeping in mind of the situations where it can be applied.

2.3 Drawbacks of the Landauer Approach

- The problem with this approach is that there is no way to obtain information about the past within this theory. We are only able to access the long time solution. The steady state approximation described before deliberately loses all initial correlations.

- Dealing with the interactions and inelastic effects seems to be difficult within this approach. Non-equilibrium Green's functions approach seems to be more transparent, in this regard.

- There is an inherent assumption that any kind of dephasing and relaxation of the electronic state takes place only in the reservoirs. Interaction of electrons with the lattice degrees of freedom giving rise to Joule heating can therefore be not handled within this approach unless this assumption is relaxed.

- The scatterer is treated like a black-box and all its effects are dumped into the scattering matrix.

2.4 Open Questions

- Is it obvious that a steady state will be reached and the electron will equilibrate only at the reservoirs? Can there be no fluctuations in these non-equilibrium steady states?

- How do we deal with interacting electrons or interactions between electrons and phonons?

Chapter 3

Calculating the Transmission Functions

In this chapter I intend to calculate the transmission probabilities of the electronic wavefunctions as functions of its energy. The method we adopt was proposed by T. Ando [29, 15]. It is based upon wave function matching at the boundaries. In this regard I would like to mention that, transmission through an atomic wire consisting of a finite scattering region have been attempted to be solved by semiemperical methods [32, 33, 34, 35]. However in these approaches there exists approximations regarding the atomic structure of the leads. Generally jellium electrodes are considered and wave functions are calculated by the transfer matrix method [36, 37] or by the Lippman-Shwinger method [38, 39, 40]. Alternatively one can use the Green's function approach [41]. However, the scheme of wave function matching proposed by Ando [29], neither requires the explicit calculation of wave functions nor does it require the calculation of the Green's functions. Besides as it will turn out that this approach is only an O(N) technique, computationally, where N is the number of

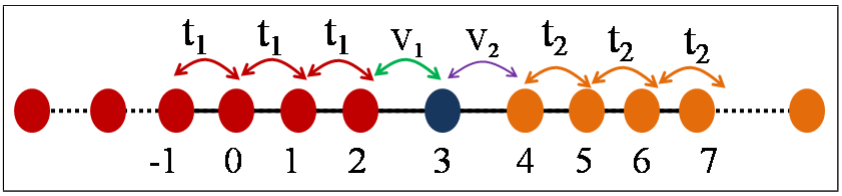

Figure 3.1: The system consists of a chain of atoms. The different kinds are represented by different colours and different values of the hopping parameters.

atoms in the scatterer.

The scatterer is treated explicitly by a recursive technique. In this chapter I will demonstrate the use of the above technique for the simplest case of a chain of atoms comprising of one or more than one impurity scatterer(s).

3.1 Introduction

Let us consider a perfectly 1-D chain of atoms comprising of monoatomic unit cells, as shown in 3.1. One can understand from the figure that I have considered two atoms of the respective leads to form a part of the scatterer. The wave function of an electron passing through this system, in the site basis, is,

$$|\psi\rangle = \sum_{j=-\infty}^{\infty} C_j|j\rangle \tag{3.1}$$

where, C_j is the amplitude of the electronic wave function at the jth site. The time independent Schrödinger equation reads as,

$$\begin{aligned} & \mathcal{H}|\psi\rangle = E|\psi\rangle \\ \Rightarrow \quad & \mathcal{H}\sum_j C_j|j\rangle = E\sum_j C_j|j\rangle \end{aligned}$$

where, $\mathcal{H}$ is the Hamiltonian of the electronic system in the site representation.

$$\therefore [E\delta_{jj'} - \mathcal{H}_{jj'}]C_j = 0 \tag{3.2}$$

(3.2) is for a particular site j'. Likewise we are supposed to get an infinite set of equations for $j' \in [-\infty, \infty]$. However apart from these infinite set of equations we also have the constraint equations for the leads. These are nothing but the Bloch conditions, assuming the leads to ideally periodic. This helps us in eliminating most of the above set of equations and define the effect of the electronic wavefunctions, in the leads as boundary conditions, exactly the way the Landauer approach does.

3.2 Recursion Relations

In order to obtain the recursion relations I shall first deal with the leads which are ideal to set up the boundary conditions for the electronic wavefunction inside the scatterer.

3.2.1 Ideal Wires

Use of Bloch condition An ideal wire is defined by the presence of a perfectly periodic potential along the length of the wire. In such a periodic system the wave functions in the adjacent cells (which are the atomic sites in my case) is related by the Bloch condition,

$$C_j = \lambda C_{j-1} \tag{3.3}$$

Also (3.2) gives us,

$$(E - \epsilon_j)C_j - tC_{j-1} - tC_{j+1} = 0 \tag{3.4}$$

where, ϵ_j is the onsite energy at the jth site. So, for the ideal leads, we have two equations, (3.3) and (3.4). These two equations can give us the value of λ for different values of energy E. On substituting for C_{j-1} and C_{j+1} in (3.4), we get,

$$\lambda = \frac{(E - \epsilon_j) \pm \sqrt{(E - \epsilon_j)^2 - 4t^2}}{2t} \tag{3.5}$$

This is also equivalent to solving the following eigenvalue equation,

$$\lambda \begin{pmatrix} C_j \\ C_{j-1} \end{pmatrix} = \begin{pmatrix} \frac{E-\epsilon_j}{t} & -1 \\ 1 & 0 \end{pmatrix} \begin{pmatrix} C_j \\ C_{j-1} \end{pmatrix} \tag{3.6}$$

The eigenvectors of the 2x2 matrix on the R.H.S of (3.6) will give the solution of C_j for the value of λ given by (3.5). Also it should be noted that for our system the above method is applicable only upto $j \leqq -1$, because, $\lambda C_0 \neq C_1$.

We need the incident wave at the boundaries of the scatterer. The boundaries are formed by the 0th cell/site on the left and the 6th cell/site on the right. A wave going from the 0th site to the 1st site is supposed to get scattered off the 1st site and hence, the amplitudes of the electronic wavefunctions at the sites $j \leqq 0$ should consist of a right going (+) (incident) and a left going (-) (reflected) amplitude. So,

$$C_j = C_j(+) + C_j(-)$$

So, the solution we get for C_j from (3.6) should consist of a left going and a right going part. Indeed reference [31] tells us that the eigenvalues λ corresponding to left and right going solutions come in pairs.

Suppose the solutions are $u(+)$ and $u(-)$ respectively, then we have for our simple case, $C_{-1} = u(+) + u(-)$ and by the Bloch condition, $C_0(\pm) = \lambda(\pm)C_{-1}(\pm)$. So,

$$C_0 = \lambda(+)u(+) + \lambda(-)u(-) \tag{3.7}$$

Also the wave incident at the right junction between the scatterer and the ideal lead gets reflected into the scattering system and only right going waves can be found in the right lead. Hence, $C_{N+1} = C_{N+1}(+)$ where N is the number of atoms in the scatterer. Similar to the solution of (3.6) for the left lead, we need to find out the λ for the right lead. Let us call it λ'.

3.2.2 Scattering Region

In the scattering we no longer have the Bloch condition and hence require to solve (3.2) via the following recursion relations:

$$E - \epsilon_0 C_0 - t_1 C_1 - t_1 C_{-1} = 0 \tag{3.8}$$

$$\begin{pmatrix} E-\epsilon_1 & -t_1 & 0 & 0 & 0 \\ -t_1 & E-\epsilon_2 & -V_1 & 0 & 0 \\ 0 & -V_1 & E-\epsilon_3 & -V_2 & 0 \\ 0 & 0 & -V_2 & E-\epsilon_4 & -V_1 \\ 0 & 0 & 0 & -t_2 & E-\epsilon_5 \end{pmatrix} \begin{pmatrix} C_1 \\ C_2 \\ C_3 \\ C_4 \\ C_5 \end{pmatrix} = \begin{pmatrix} t_1 C_0 \\ 0 \\ 0 \\ 0 \\ t_2 C_6 \end{pmatrix} \tag{3.9}$$

$$E - \epsilon_6 C_6 - t_2 C_7 - t_2 C_5 = 0 \tag{3.10}$$

We are interested in finding out the transmission probability. So, we should be concerned with the propagation of $C_0(+)$ across the scatterer. Also, $C_7 = \lambda'(+)C_6(+)$

and $C_6(+) = C_6 = TC_0(+)$. Solving the above set of equations would then give us T.

3.3 Method

The above scheme is implemented numerically as will be described in this section. It should be mentioned that this implementation is just in its infancy stage. We have done calculations for a perfectly one dimensional atomic chain. The scattering region consists of afew number of atoms. The idea was to see if it is possible to get a transmission function that might resemble the lorentzian form used in the previous chapter.

So we tuned the onsite energies of the atoms in the chain to mimic the effect of scattering in the most minimal level. In order to implement the scheme numerically I performed the following steps:

1. The first step involved calculation of eigenvalues and eigenvectors corresponding to equation (3.6). The represents the situation in ideal wires or ideal leads, between which the impurity region is sandwiched. The expressions were found out analytically (for a 2x2 matrix) and were implemented in a Fortran 90 code.

2. As a first check the Bloch wave vectors were obtained and plotted as a function of energy representing travelling waves, i.e. k_x values were plotted from 0 to π/a. They indeed turned out to be like the ones obtained from a tight-binding Hamiltonian. We need to consider only the imaginary eigenvalues of (3.6). These eigenvalues represent the travelling waves that are transmitted across the impurity region. Figure(3.2) shows the classification of travelling and

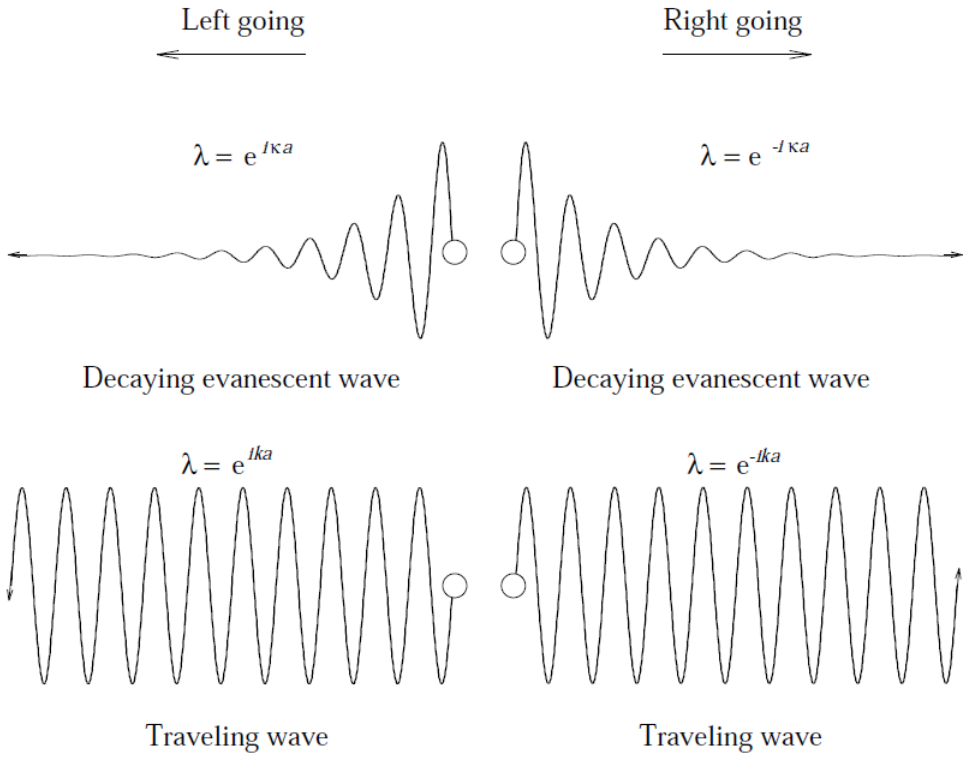

Figure 3.2: This figure shows the four types of waves that correspond to the eigenvalue λ in (3.6).

evanescent waves, used in this scheme. The wave vectors obtained by solving (3.6) is shown in figure(3.3).

3. Let us suppose that the atoms 1-5 shown in figure (3.1) are the impurity atoms. Then, we know that the electron on atom 6 will only have a right going component. So, I used the wavefunction at site 7, i.e. $C_7 = u(+)$, the eigenvectors obtained from the first step. Thus C_6 was found out by the Bloch condition and supplied to the recursion relation obtained in the previous section. This relation was used to get the wavevectors until C_{-1}.

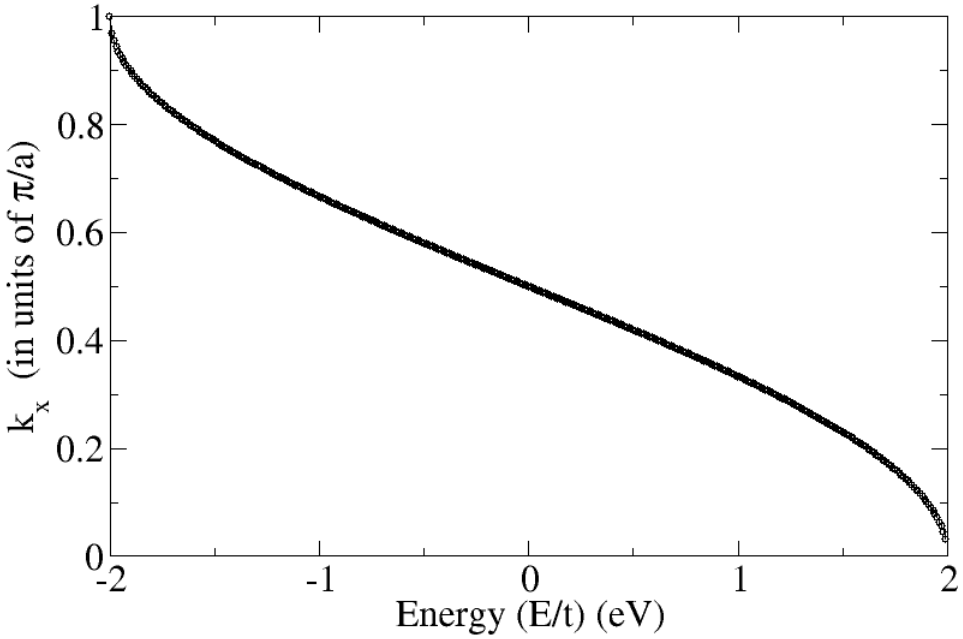

Figure 3.3: Bloch wave vectors are plotted as a function of energy. These are obtained by solving the eigenvalue equation in (3.6).

4. $C_0(+)$ was calculated using the relation,

$$C_0(+) = \frac{C_{-1} - e^{ik}}{e^{-ik} - e^{ik}},$$

to finally get, $T(\epsilon) = \frac{|C_6|}{|C_0(+)|}$.

3.4 Results

In order to do the calculations we have set the following parametric situation:

- We have used a finite number of atoms inside the impurity scatterer.

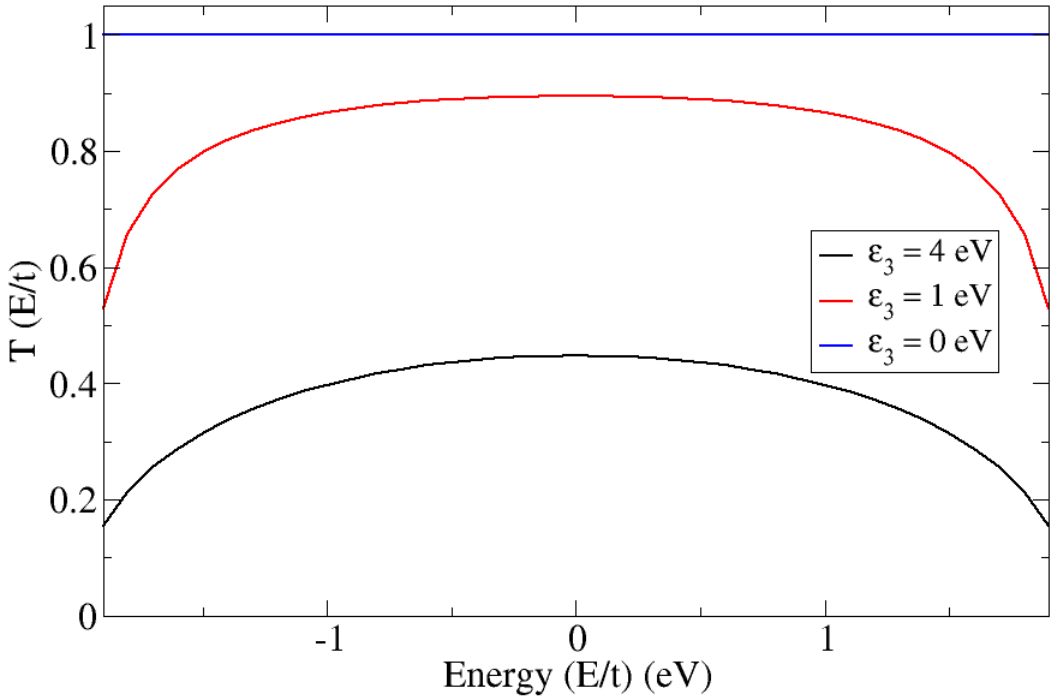

Figure 3.4: Transmission function calculated for a 1−D chain of atoms. This is the case of a single impurity where the onsite scattering potential of the atom 3 in the impurity region is varied.

- For an ideal wire the onsite energies on all the sites was set to $\epsilon_j = 0$ eV, where j is the atomic site. This is basically to represent a scattering free region. That is why as expected we get,

$$T(\epsilon) = 1.$$

- **Single impurity**: To see the effect of presence of impurities I have first set the atom number 3 in figure(3.1) to have an onsite energy equal to something different from 0 eV. So, we did calculations for ϵ_3 =0 eV, 2 eV, 4 eV. As can be seen from the figures, the transmission is approximately flat for any impurity

onsite energy. The only effect of the impurity was to change the value of $T(\epsilon)$. The higher the site energy, lower is the value of $T(\epsilon)$, which is as expected.

- The above two observations are presented in figure(3.4).

- Now, we change the situation by treating all the 5 atoms as impurity, i.e. now I have a 5-atom scattering region. We see non-trivial features in the transmission function for this situation, and that is again expected because now the effect of scattering has increased. The transmission function develops a peak around a certain energy value. This indeed represents the peak like feature we are motivated for. This is shown in figure(3.5).

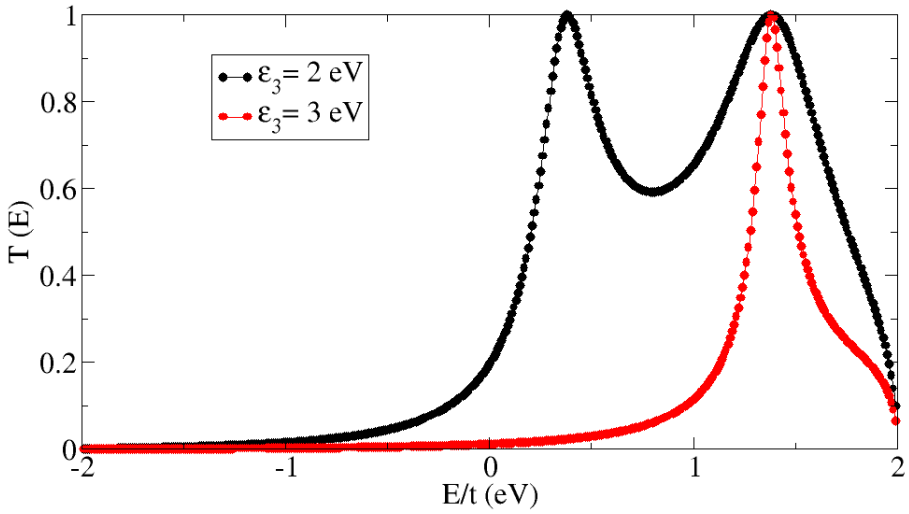

Figure 3.5: Transmission function calculated for a 1−D chain of atoms. In this case, we have considered a 5 atom impurity region. All the 5 atoms have the same effect of scattering.

- In order to further play with the transmission function we associated different scattering effects on different atoms in the 5-atom scattering region. The transmission function is now high in some energy range and also goes to a

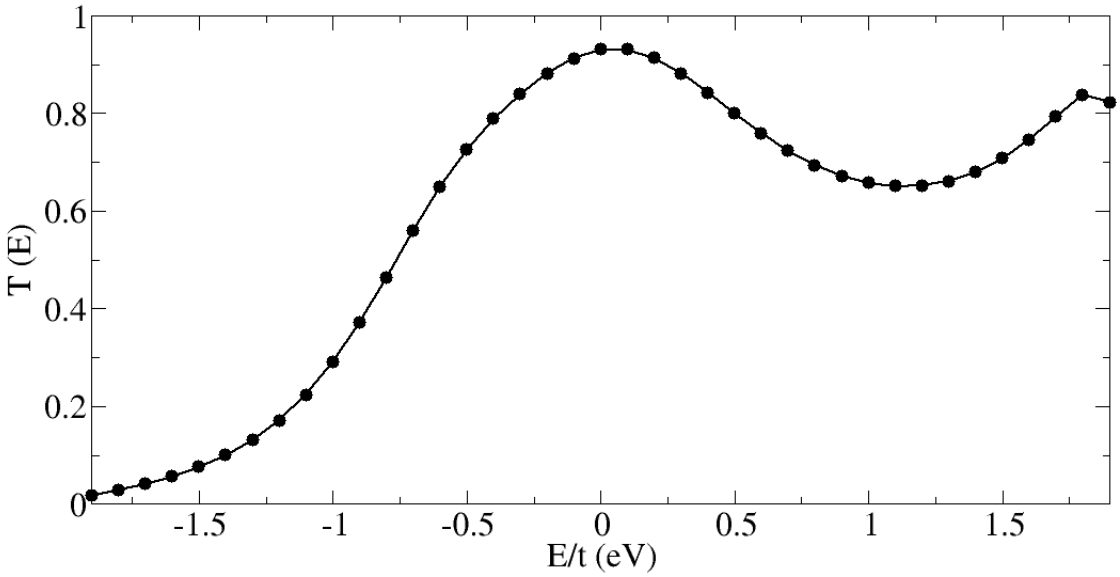

Figure 3.6: Transmission function calculated for a 1−D chain of atoms. In this case, we have associated different effects of scattering in the impurity region by associating different onsite potential energies.

minima in some other energy range. This suggests that the transmission can be a non-trivial function of energy and it depends on how the impurity scatterers are situated. This is depicted in figure(3.6). Hence it is not always relevant to use flat transmission functions for such one dimensional nanowire geometries.

3.5 Conclusion

- We learnt from Chapter 1 that in the Landauer-Büttiker formalism all information about the scattering region is buried inside the transmission function.

- However, the Landauer-Büttiker formalism does not provide us with any scheme to calculate the transmission function.

- So, in this chapter, we tried to calculate the transmission function as a function of energy using a real space wave function matching technique.

- We observed that presence of impurity defects in the scattering region can greatly alter the form of the transmission function. This is of particular importance in systems like carbon nanotubes. These systems have a high concentration of defects and hence a flat transmission function is not desired to be used for calculation of the transport calculations.

- Here, we have only seen the effect of onsite disorder. Effect of bond disorder is not analysed. Bond disorder would imply tuning the hopping parameter t_j in the tight binding Hamiltonian.

- We intend to go beyond a $1-$D chain of atoms and utilize the scheme mentioned in this chapter for calculating transmission functions for different kinds of geometries like quantum point contacts or nanotubes and use them for our future calculations.

Chapter 4

Joule Heating in nanoscale junctions: A Discussion of experiments and theory

This chapter attempts to briefly survey the state of art in theory and experiments relevant to the issue of local heating in atomic scale contacts. The development of theory for a description of Joule heating is one of the main objectives of my project. This project is motivated by the fact that an understanding of local heating or hot spots and how to mitigate them is very important in modeling a realistic nanoscale device. Experiments on nanoscale junctions [42, 43] suggest local heating with increasing electrical current. At a first glance this seems to be surprising because the size of the contacts is much smaller than the electron mean free path and so scattering is not expected. However as Todorov [9, 45, 58, 57] and Di Ventra [46] argue that this is not surprising if one considers the huge electron current density that appears at the junctions.

It is now established that large current densities in nanosystems can lead to substantial heating compared to their bulk counterparts. These observations can be found in [47, 48, 49]. According to Todorov[9], this phenomena of self heating happens even if the contacts are ideal. The contacts may be ballistic for the electrons but not for the phonons, and, also the electrons are highly energetic compared to the phonons. Let us frame the argument in the following way: When a high density non-equilibrium electron gas (liquid) flows across a nanoscale junction, most naturally it interacts with the atomic oscillators at the junction simply because of the difference in energy. So the steady state oscillator temperature (so that there is no energy flow between the oscillator and the electrons) is different from the ambient temperature. It should be noted that Todorov considered a one way transfer of energy, namely from the electrons to the phonons.

But as Di Ventra argues in [46], large electron current will also lead to increased Coulomb interactions and if that is the case then the electrons are expected to equilibrate at a different effective temperature. This is because electrons do not always behave as an electron gas. If the electrons are treated as a viscous liquid[51], then increase in electron density will give rise to an increase in electron-electron Coulomb repulsion. Besides if we consider two way transfer of energy then the temperature of the oscillator (T_{osc}) should be equal to the electronic temperature (T_{e}). Hence the temperature that should enter the Fermi-Dirac distribution of the electrons should be different from the ambient temperature. This is exactly what is done in the calculations of Chapter 2. Also, the local electronic temperature is going to affect the electron-phonon scattering. An approximate argument shows that T_{ion} is proportional to $V^{1/2}$, where V is the applied bias[9, 47, 48, 49, 50].

These considerations may be further augmented by a recent experiment conducted by Daniel R. Ward *et. al.* of Rice University [55]. By surface enhanced Raman emission they determined effective temperatures for both the oscillator vibrational modes and the electrons, pertaining to a biased metallic nanoscale junction.

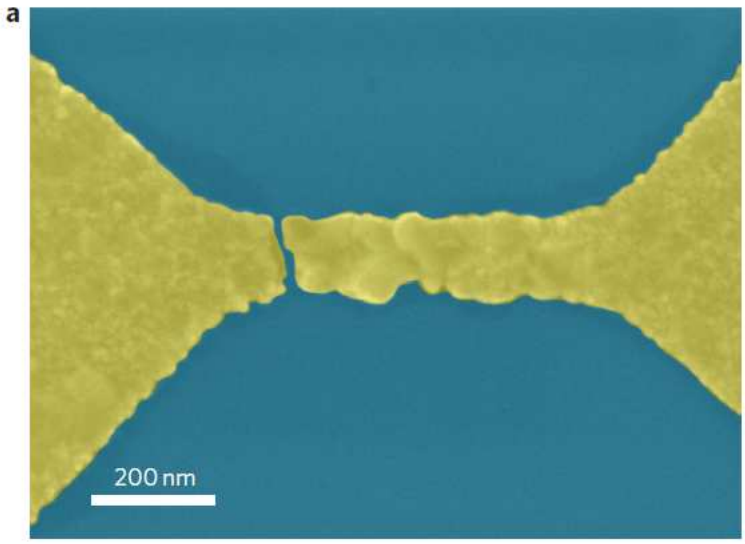

Figure 4.1: Schematic of a nanogap used in the experiment by Ward *et. al.*. Ref: Nature Nanotechnology, Vol. 6 (33).

They mention that the electronic distribution rethermalizes on a scale set by inelastic electron-electron interactions. As I have mentioned in Chapter 2, the Landauer-Büttiker approach assumes that the thermalization of the electrons take place far away from the junctions, in the reservoirs; so the source and drain electrodes have identical temperatures. But this experiment shows that this is not the necessary case. Electron-phonon scattering also comes into action to transfer energy to the lattice, such that the lattice develops a temperature over a thermodynamic extent, and, the electrons can rethermalize in the electrodes itself. Hence, it is not necessary to incorporate the same temperature for the electrons that enter the scat-

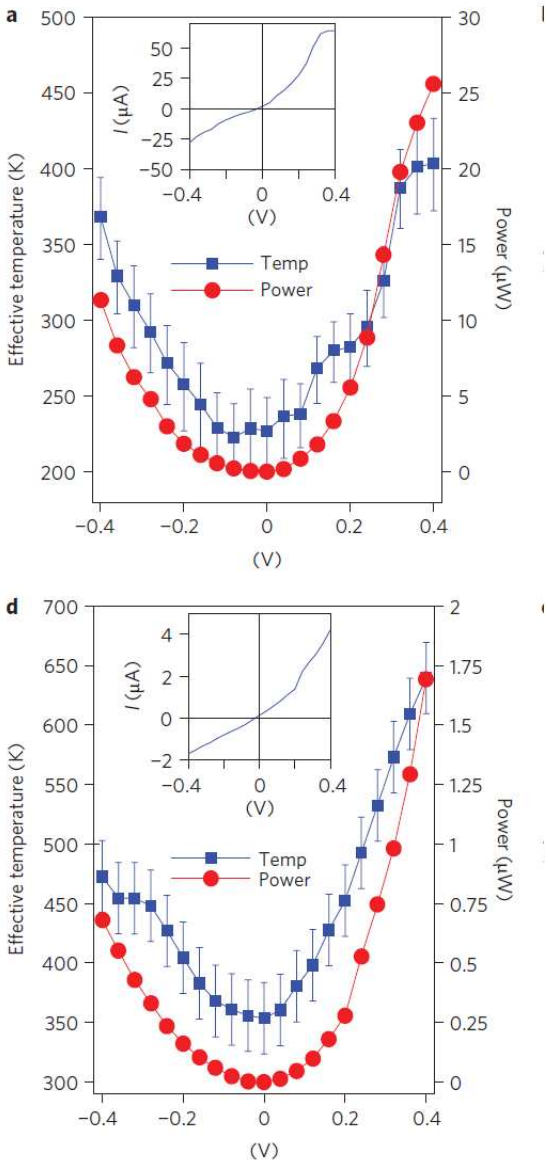

Figure 4.2: This figure is again taken from Nature Nanotechnology, Vol. 6 (33), with respect to the experiment conducted by Ward *et. al.*. It shows the effective temperature of the electron and the dissipated power as a function of the bias voltage. Inset shows the IV characteristic and a nonlinearity and asymmetric current can be observed with respect to voltage polarity.

terer from the left and the right reservoir. Figure(4.2) shows the experimental result that indicates electron rethermalization.

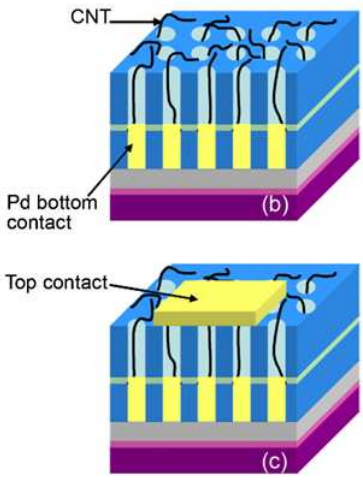

Figure 4.3: This figure is taken from the experiment conducted by Sayer *et. al.* IEEE Transactions on Components and Packaging Technologies, Vol. 33, No. 1. It shows a schematic of the experimental set up that was used. The nanotubes were 400 nm long and 10 nm in diameter.

It should also be remarked that the junction heating also depends strongly on the transmittivity of the junctions for both charge and energy current. In this regard, study of thermal transport at nanoscale becomes important. Also, regarding the structure of the junction, the experimental set up that first caught our attention was of Sayer *et.al.* at Purdue University [56]. This experimental set up consisted of single walled carbon nanotube devices grown from within porous anodic alumina substrate. Figure(4.3) shows the set up and it is clear that the junctions are highly asymmetric. Thereby, one requires to properly model the junctions keeping in mind that the presence of impurity can highly alter the energy dependence of the transmission function (as shown in Chapter 3). Another consequence of junction heating is embrittlement of wires[57]. The combined effect of all these phenomena can lead to unexpected observations. In fact, experimentally it has been observed that Au-single atom contacts and chains break at applied voltages of 1 to 2V [60, 61, 62, 63].

This implies the onset of bond disorder due to heating. And hence, in such situations another issue comes into action, namely the efficiency of thermal transport in nanoscale junctions[53, 64, 54].

In this chapter, I have attempted to highlight the subtle issues that one should keep in mind to model self heating in nanoscale junctions. By discussing the experiment in [55], I tried to justify the relevance of considering two different temperatures for the left and right leads.

Di Ventra suggests in [46] that the local increase of electronic temperature in a nanojunction can be extracted from Johnson-Nyquist noise[52]. And if that is the case, then the T_e entering in the Fermi-Dirac distribution function of the electron is definitely not the temperature of the reservoir. An extensive theoretical model taking care of both electron-electron interactions and electron-phonon interactions still remains a challenge in this field. A proper correlation between experiments and existing theory also needs to be done. We intend to look into these aspects as far as possible, in our future projects.

Appendices

Appendix A

Current operator using second quantized notation

Use of second quantization particularly organizes our task in formulation of the scattering problem by inherently taking care of the quantum statistics of the current carriers. many electrons can populate the transverse modes in the leads and the effect of Pauli Exclusion principle is easily taken care of by the anticommutation relations of the incoming and outgoing state operators. The strategy involves writing the equations in terms of ceratin field operators. These operators, operate in space and time and physically represent the presence or absence of a paticle in position $\vec{r}$. They can be written in terms of the incoming and outgoing channel operators as the following:

$$\hat{\psi}_{in}(\vec{r},t) = \sum_{nk} \phi^{in}_{kn}(\vec{r},t)\ \ \hat{a}_{kn}$$
$$\hat{\psi}_{out}(\vec{r},t) = \sum_{nk} \phi^{out}_{kn}(\vec{r},t)\ \ \hat{b}_{kn}$$

$\phi^{in(out)}_{kn}(\vec{r},t)$: Incoming (outgoing) states with wave vector $\vec{k}$ in channel n.

$\hat{a}_{kn}(\hat{b}_{kn})$: Annihilation operator for an incoming(outgoing) state.

$$\sum_k \qquad\qquad : \int \ \mathrm{d}k \ D(\vec{k})$$

Hence, I can write the field operator in the left lead (α) as,

$$\hat{\psi}_\alpha(\vec{r},t) = \frac{1}{\sqrt{L_x}} \int \mathrm{d}\epsilon \ e^{-i\epsilon t/\hbar} \ \sum_{n=1}^{N_\alpha} \left(\hat{a}_{\alpha n}(k) e^{ikx} + \hat{b}_{\alpha n}(k) e^{-ikx} \right) \ \frac{\chi_{\alpha n}(\vec{r_\perp}) \ L_x}{2\pi\hbar \ v_{\alpha n}(\epsilon)}$$

Let us write,

$$\begin{aligned} \hat{a}_{\alpha n}(\epsilon) =& \frac{\hat{a}_{\alpha n}(k)}{\sqrt{L_x} \ \sqrt{2\pi\hbar \ v_{\alpha n}}} \\ \hat{b}_{\alpha n}(\epsilon) =& \frac{\hat{b}_{\alpha n}(k)}{\sqrt{L_x} \ \sqrt{2\pi\hbar \ v_{\alpha n}}} \end{aligned}$$

After substitution of the above opeartors in the field operator forms for the left(α) and the right(β) leads, we get,

$$\begin{aligned} \hat{\psi}_\alpha(\vec{r},t) =& \sum_{n=1}^{N_\alpha} \int \mathrm{d}\epsilon \ \frac{L_x}{\sqrt{2\pi\hbar \ v_{\alpha n}(\epsilon)}} \left(\hat{a}_{\alpha n}(\epsilon) e^{ikx} + \hat{b}_{\alpha n}(\epsilon) e^{-ikx} \right) \chi_{\alpha n}(\vec{r_\perp}) \\ \hat{\psi}_\beta(\vec{r},t) =& \sum_{n=1}^{N_\beta} \int \mathrm{d}\epsilon \ \frac{L_x}{\sqrt{2\pi\hbar \ v_{\beta n}(\epsilon)}} \left(\hat{a}_{\beta n}(\epsilon) e^{ikx} + \hat{b}_{\beta n}(\epsilon) e^{-ikx} \right) \chi_{\beta n}(\vec{r_\perp}) \end{aligned}$$

Now, the current operator in the left lead is given as,

$$\boxed{\hat{I}_\alpha(x,t) = \frac{\hbar e}{2im} \int \mathrm{d}\vec{r}_\perp \left[\hat{\psi}^\dagger_\alpha(\vec{r},t) \left(\frac{\partial}{\partial x} \hat{\psi}_\alpha(\vec{r},t) \right) - \left(\frac{\partial}{\partial x} \hat{\psi}^\dagger_\alpha(\vec{r},t) \right) \hat{\psi}_\alpha(\vec{r},t) \right]} \qquad \text{(A.1)}$$

Substitution of the forms of $\hat{\psi}_\alpha(\vec{r},t)$ into $\hat{I}_\alpha(x,t)$ and assuming that v, k, are independent of energy and scales of the order of the Fermi energy, we get,

$$\boxed{\hat{I}_\alpha(t) = \frac{e}{2\pi\hbar} \sum_n \int \mathrm{d}\epsilon \ \mathrm{d}\epsilon' \ e^{i(\epsilon-\epsilon')t/\hbar} \left[\hat{a}^\dagger_{\alpha n}(\epsilon) \hat{a}_{\alpha n}(\epsilon') - \hat{b}^\dagger_{\alpha n}(\epsilon) \hat{b}_{\alpha n}(\epsilon') \right]} \qquad \text{(A.2)}$$

The operators $\hat{a}_{\alpha n}(\epsilon)$ and $\hat{b}_{\alpha n}(\epsilon)$ are related via the scattering matrix ,

$$\begin{pmatrix} \hat{b}_{\alpha 1} \\ \hat{b}_{\alpha 2} \\ \vdots \\ \hat{b}_{\alpha N_\alpha} \\ \vdots \\ \hat{b}_{\beta N_\beta} \end{pmatrix} = S \begin{pmatrix} \hat{a}_{\alpha 1} \\ \hat{a}_{\alpha 2} \\ \vdots \\ \hat{a}_{\alpha N_\alpha} \\ \vdots \\ \hat{a}_{\beta N_\beta} \end{pmatrix}$$

where, the scattering matrix for a 2 terminal device is represented in terms of block matrices, $(S_{\gamma\delta})$, (γ, δ can be α or β), as the following:

$$\begin{pmatrix} S_{\alpha\alpha} & S_{\alpha\beta} \\ S_{\beta\alpha} & S_{\beta\beta} \end{pmatrix} \tag{A.3}$$

$(S_{\alpha\alpha})_{ij}$	Responsible for **reflection** of a carrier in the incoming state in lead 1 channel i, to an outgoing state in lead 2, channel j.
$(S_{\alpha\beta})_{ij}$	Responsible for **transmission** of a carrier in the incoming state in lead 1, channel i, to an outgoing state in lead 2, channel j.
$(S_{\beta\alpha})_{ij}$	Responsible for **transmission** of a carrier in the incoming state in lead 2, channel i, to an outgoing state in lead 1, channel j.
$(S_{\beta\beta})_{ij}$	Responsible for **reflection** of a carrier in the incoming state in lead 2, channel i, to an outgoing state in lead 2, channel j.

Based on the above I can write,

$$\sum_{n} \hat{b}^{\dagger}_{\alpha n}(\epsilon)\hat{b}_{\alpha n}(\epsilon') = \sum_{\substack{\gamma\delta \\ kp}} \hat{a}^{\dagger}_{\gamma k}(\epsilon) \left(S^{\dagger}_{\alpha\gamma}S_{\alpha\delta}\right)_{kp} \hat{a}_{\delta p}(\epsilon') \tag{A.4}$$

$$\sum_{n} \hat{a}^{\dagger}_{\alpha n}(\epsilon)\hat{a}_{\alpha n}(\epsilon') = \sum_{\substack{\gamma\delta \\ kp}} \hat{a}^{\dagger}_{\gamma k}(\epsilon)\hat{a}_{\delta p}(\epsilon')\delta_{\alpha\gamma}\delta_{\beta\delta}\delta_{kp} \tag{A.5}$$

Therefore,

$$\hat{I}_{\alpha}(t) = \frac{e}{2\pi\hbar} \sum_{\substack{\gamma\delta \\ kp}} \int \mathrm{d}\epsilon \;\; \mathrm{d}\epsilon' \;\; e^{i(\epsilon-\epsilon')t/\hbar} \;\; \left\langle \hat{a}^{\dagger}_{\gamma k}(\epsilon) A^{kp}_{\gamma\delta}(\alpha;\epsilon,\epsilon')\hat{a}_{\delta p}(\epsilon') \right\rangle$$

where,

$$A^{kp}_{\gamma\delta}(\alpha;\epsilon,\epsilon') = \delta_{\alpha\gamma}\delta_{\alpha\delta}\delta_{kp} - \left(S^{\dagger}_{\alpha\gamma}S_{\alpha\delta}\right)_{kp}$$

For a non-interacting system,

$$\left\langle \hat{a}^{\dagger}_{\gamma k}(\epsilon)\hat{a}_{\delta p}(\epsilon') \right\rangle = \delta_{\alpha\gamma}\delta_{kp}\delta(\epsilon-\epsilon')f_{\gamma}(\epsilon)$$

Hence,

$$\boxed{\left\langle \hat{I_{\alpha}}(t) \right\rangle = \frac{e}{2\pi\hbar} \int \mathrm{d}\epsilon \;\; \sum_{\gamma k} A^{kk}_{\gamma\gamma}(\alpha;\epsilon,\epsilon) \;\; f_{\gamma}(\epsilon)} \tag{A.6}$$

Now,

$$A^{kk}_{\gamma\gamma}(\alpha;\epsilon,\epsilon) = N_{\alpha} - \sum_{\gamma} \mathrm{Tr}\left(S^{\dagger}_{\alpha\gamma}S_{\alpha\gamma}\right)$$

So, for a 2-terminal device,

$$\begin{aligned}
&\left[N_\alpha - \sum_\gamma \mathrm{Tr}\left(S^\dagger_{\alpha\gamma} S_{\alpha\gamma}\right)\right] \; f_\gamma(\epsilon) \\
&= \left[N_\alpha - \mathrm{Tr}\left(S^\dagger_{\alpha\alpha} S_{\alpha\alpha}\right)\right] \; f_\alpha(\epsilon) - \mathrm{Tr}\left(S^\dagger_{\alpha\beta} S_{\alpha\beta}\right) \; f_\beta(\epsilon) \\
&= \mathrm{Tr}\left(S^\dagger_{\alpha\beta} S_{\alpha\beta}\right)\left[f_\alpha(\epsilon) - f_\beta(\epsilon)\right] \\
&= \sum_n T_n(\epsilon) \; \left[f_\alpha(\epsilon) - f_\beta(\epsilon)\right]
\end{aligned}$$

Therefore,

$$\boxed{\left\langle \hat{I}_\alpha(t) \right\rangle = \frac{e}{2\pi\hbar} \int_0^\infty \mathrm{d}\epsilon \; \sum_n T_n(\epsilon) \; \left[f_\alpha(\epsilon) - f_\beta(\epsilon)\right]} \tag{A.7}$$

Appendix B

Properties of the Scattering Matrix

Here I demonstrate the two properties of the scattering matrix of a two terminal device. A slight thought would tell us that this is general for an N terminal device also. Let us refer back to (A.3), (A.4), (A.5).

Flux conservation demands,

$$\left\langle n_\alpha^{\text{out}} + n_\beta^{\text{out}} \right\rangle = \left\langle n_\alpha^{\text{in}} + n_\beta^{\text{in}} \right\rangle$$

or,

$$\left\langle \sum_{\substack{\gamma\delta \\ kp}} \hat{a}_{\gamma k}^\dagger \left(S_{\alpha\gamma}^\dagger S_{\alpha\delta} + S_{\beta\gamma}^\dagger S_{\beta\delta} \right)_{kp} \hat{a}_{\delta p} \right\rangle = \sum_{\substack{\gamma\delta \\ kp}} \delta_{\gamma\delta}\delta_{kp} \left\langle \hat{a}_{\gamma k}^\dagger \hat{a}_{\delta p} \right\rangle \tag{B.1}$$

So, only for $\gamma = \delta$ and $k = p$, there corresponds a non-zero term on the R.H.S. of (B.1) and it is equal to f_δ.

So, we have,

$$S^{\dagger}_{\alpha\alpha}S_{\alpha\alpha} + S^{\dagger}_{\beta\alpha}S_{\beta\alpha} = \mathbb{1}_{\alpha}$$

$$S^{\dagger}_{\alpha\beta}S_{\alpha\beta} + S^{\dagger}_{\beta\beta}S_{\beta\beta} = \mathbb{1}_{\beta}$$

$$S^{\dagger}_{\alpha\alpha}S_{\alpha\alpha} + S^{\dagger}_{\beta\alpha}S_{\beta\alpha} = 0$$

$$S^{\dagger}_{\alpha\alpha}S_{\alpha\beta} + S^{\dagger}_{\beta\alpha}S_{\beta\beta} = 0$$

This is the same as,

$$\boxed{S^{\dagger}S = \mathbb{1}} \quad : \text{Unitary} \tag{B.2}$$

Time reversal symmetry demands,

$$\boxed{S = S^{T}} \quad : \text{Symmetric} \tag{B.3}$$

Appendix C

Mathematical Steps Involved in obtaining $P_{\alpha\beta}(0)$

The noise power is represented as,

$$P_{\alpha\beta}(\omega) = 2\int_{-\infty}^{\infty}\Big[\underbrace{\langle I_\alpha(t)I_\beta(t')\rangle}_{1} - \underbrace{\langle I_\alpha(t)\rangle\langle I_\beta(t')\rangle}_{2}\Big]e^{i\omega(t-t')}\mathrm{d}(t-t') \tag{C.1}$$

C.1 Step 1

Term(1) will involve the following:

$$\sum_{\substack{\gamma\delta\\kp}}\sum_{\substack{\lambda\nu\\mn}}\Big\langle \hat{a}^\dagger_{\gamma k}(\epsilon_1)\ A^{kp}_{\gamma\delta}(\alpha;\epsilon_1,\epsilon_2)\ \hat{a}_{\delta p}(\epsilon_2)\ \hat{a}^\dagger_{\lambda m}(\epsilon_3)\ A^{mn}_{\lambda\nu}(\beta;\epsilon_3,\epsilon_4)\ \hat{a}_{\nu n}(\epsilon_4)\Big\rangle$$

$$=\sum_{\substack{\gamma\delta\\kp}}\sum_{\substack{\lambda\nu\\mn}}A^{kp}_{\gamma\delta}(\alpha;\epsilon_1,\epsilon_2)\ A^{mn}_{\lambda\nu}(\beta;\epsilon_3,\epsilon_4)\ \Big\langle \hat{a}^\dagger_{\gamma k}(\epsilon_1)\ \hat{a}_{\delta p}(\epsilon_2)\ \hat{a}^\dagger_{\lambda m}(\epsilon_3)\ \hat{a}_{\nu n}(\epsilon_4)\Big\rangle$$

For a non-interacting system,

$$\left\langle \hat{a}_1^\dagger \hat{a}_2 \hat{a}_3^\dagger \hat{a}_4 \right\rangle = \left\langle \hat{a}_1^\dagger \hat{a}_2 \right\rangle \left\langle \hat{a}_3^\dagger \hat{a}_4 \right\rangle + \delta_{14}\delta_{23} f_1 \left(1 - f_2\right)$$

$$1 : \gamma, k, \epsilon_1 \quad ; \quad 2 : \delta, p, \epsilon_2$$

$$3 : \lambda, m, \epsilon_3 \quad ; \quad 4 : \nu, n, \epsilon_4$$

On substituting (A.1), Term(2) gets cancelled and we are left with,

$$P_{\alpha\beta}(\omega) = \frac{2e^2}{h^2} \int_0^\infty \Bigg(\int_{-\infty}^{\infty} \sum_{\substack{\gamma\delta \\ mn}} A_{\gamma\delta}^{mn}(\alpha; \epsilon, \epsilon') \;\; A_{\delta\gamma}^{nm}(\beta; \epsilon', \epsilon) \\ f_\gamma(\epsilon)\big(1 - f_\delta(\epsilon')\big) \;\; e^{\frac{i(\epsilon-\epsilon')(t-t')}{\hbar}} \;\; e^{i\omega(t-t')} \;\; \mathrm{d}(t-t') \Bigg) \;\; \mathrm{d}\epsilon$$

or,

$$P_{\alpha\beta}(\omega) = \frac{2e^2}{h^2} \int_0^\infty \Bigg(\sum_{\substack{\gamma\delta \\ mn}} A_{\gamma\delta}^{mn}(\alpha; \epsilon, \epsilon') \;\; A_{\delta\gamma}^{nm}(\beta; \epsilon', \epsilon) \\ f_\gamma(\epsilon)\big[1 - f_\delta(\epsilon')\big] \;\; \delta\big((\epsilon - \epsilon')/\hbar + \omega\big) \Bigg) \;\; \mathrm{d}\epsilon$$

or,

$$P_{\alpha\beta}(\omega) = \frac{2e^2}{h^2} \int_0^\infty \Bigg(\sum_{\substack{\gamma\delta \\ mn}} A_{\gamma\delta}^{mn}(\alpha; \epsilon, \epsilon + \hbar\omega) \;\; A_{\delta\gamma}^{nm}(\beta; \epsilon + \hbar\omega, \epsilon) \\ f_\gamma(\epsilon)\big[1 - f_\delta(\epsilon + \hbar\omega)\big] \Bigg) \mathrm{d}\epsilon \qquad \text{(C.2)}$$

C.2 Step 2

This step involves evaluation of the term:

$$\sum_{\substack{\gamma\delta\\mn}} A^{mn}_{\gamma\delta}(\alpha;\epsilon,\epsilon+\hbar\omega)\;\; A^{nm}_{\delta\gamma}(\beta;\epsilon+\hbar\omega,\epsilon)\;\; f_\gamma(\epsilon)\big[1-f_\delta(\epsilon+\hbar\omega)\big]$$

In the $\omega \longrightarrow 0$(static limit), this is,

$$\sum_{\substack{\gamma\delta\\mn}} A^{mn}_{\gamma\delta}(\alpha;\epsilon,\epsilon)\;\; A^{nm}_{\delta\gamma}(\beta;\epsilon,\epsilon)\;\; f_\gamma(\epsilon)\big[1-f_\delta(\epsilon)\big]$$

I shall omit the energy arguments from now. All energy arguments are, ϵ, unless otherwise specified. Let me define,

$$\begin{aligned}
\mathcal{I} =& \sum_{\substack{\gamma\delta\\mn}} \Big[\delta_{mn}\delta_{\alpha\gamma}\delta_{\alpha\delta} - \left(S^\dagger_{\alpha\gamma}S_{\alpha\delta}\right)_{mn}\Big] \quad \Big[\delta_{nm}\delta_{\beta\delta}\delta_{\beta\gamma} - \left(S^\dagger_{\beta\delta}S_{\beta\gamma}\right)_{nm}\Big] \quad f_\gamma\left(1-f_\delta\right) \\
=& \sum_{\substack{\gamma\delta\\mn}} \Big[\delta_{mn}\delta_{\alpha\gamma}\delta_{\alpha\delta}\delta_{\beta\delta}\delta_{\beta\gamma} - \delta_{mn}\delta_{\alpha\gamma}\delta_{\alpha\delta}\left(S^\dagger_{\beta\delta}S_{\beta\gamma}\right)_{nm} \\
& \quad - \delta_{nm}\delta_{\beta\delta}\delta_{\beta\gamma}\left(S^\dagger_{\alpha\gamma}S_{\alpha\delta}\right)_{mn} + \left(S^\dagger_{\alpha\gamma}S_{\alpha\delta}\right)_{mn}\left(S^\dagger_{\beta\delta}S_{\beta\gamma}\right)_{nm}\Big] f_\gamma\left[1-f_\delta\right] \qquad \text{(C.3)}
\end{aligned}$$

C.2.1 Case I : $\alpha = \beta = \alpha$ (say)

Let,

$$\begin{aligned}
\text{Term(i)} =& \sum_{\substack{\gamma\delta\\mn}} \delta_{mn}\delta_{\alpha\gamma}\delta_{\alpha\delta} f_\gamma\left[1-f_\delta\right] \\
=& N_\alpha \;\; f_\alpha\left[1-f_\alpha\right]
\end{aligned}$$

$$\begin{aligned}\text{Term(ii)} + \text{Term(iii)} &= -2 \ \text{Tr} \ \left(S^{\dagger}_{\alpha\alpha} S_{\alpha\alpha}\right) \ f_{\alpha}\left[1 - f_{\alpha}\right] \\ &= -2 \ f_{\alpha}\left[1 - f_{\alpha}\right]\left[N_{\alpha} - \text{Tr} \ \left(tt^{\dagger}\right)\right]\end{aligned}$$

where, I have used,

$$S^{\dagger} S = \mathbb{1}$$

and, I have defined,

$$S_{\alpha\beta} = t \quad \text{and} \quad S_{\beta\alpha} = t'$$

where, $\mathbb{1}$: Identity matrix of dimension $\left((N_{\alpha} + N_{\beta}) \ \text{X} \ (N_{\alpha} + N_{\beta})\right)$

$$\begin{aligned}\text{Term(iv)} = &\sum_{\substack{\gamma\delta \\ mn}} \left(S^{\dagger}_{\alpha\gamma} S_{\alpha\delta}\right)_{mn} \left(S^{\dagger}_{\beta\delta} S_{\beta\gamma}\right)_{nm} f_{\gamma}\left[1 - f_{\delta}\right] \\ = &\text{Tr} \ \left\{\left(S^{\dagger}_{\alpha\alpha} S_{\alpha\alpha}\right)^2\right\} \ f_{\alpha}\left[1 - f_{\alpha}\right] \\ + &\text{Tr} \ \left\{\left(S^{\dagger}_{\alpha\beta} S_{\alpha\beta}\right)^2\right\} \ f_{\beta}\left[1 - f_{\beta}\right] \\ + &\underbrace{\text{Tr} \ \left(S^{\dagger}_{\alpha\alpha} S_{\alpha\beta} S^{\dagger}_{\alpha\beta} S_{\alpha\alpha}\right) \ f_{\alpha}\left[1 - f_{\beta}\right]}_{a} \\ + &\underbrace{\text{Tr} \ \left(S^{\dagger}_{\alpha\beta} S_{\alpha\alpha} S^{\dagger}_{\alpha\alpha} S_{\alpha\beta}\right) \ f_{\beta}\left[1 - f_{\alpha}\right]}_{b}\end{aligned}$$

Now,

$$\text{Tr} \ \left\{\left(S^{\dagger}_{\alpha\alpha} S_{\alpha\alpha}\right)^2\right\} + \text{Term(ii)} + \text{Term(iii)} = \text{Tr} \ \left\{\left(S^{\dagger}_{\beta\alpha} S_{\beta\alpha}\right)^2\right\} \ f_{\alpha}\left[1 - f_{\alpha}\right]$$

and, in Term(iv), Term(a) + Term(b)

$$= \mathrm{Tr}\left\{\left(\mathbb{1}_\alpha - S_{\alpha\beta}S^\dagger_{\alpha\beta}\right) S_{\alpha\beta}S^\dagger_{\alpha\beta}\right\}\left[f_\alpha(1-f_\beta) + f_\beta(1-f_\alpha)\right]$$

Collecting all the above results, we finally converge to the following result,

$$P_{\alpha\alpha}(\omega=0) = \int_0^\infty \Big(\mathrm{Tr}\left\{\left(tt^\dagger\right)^2\right\} f_\beta\left(1-f_\beta\right) + \mathrm{Tr}\left\{\left(t't'^\dagger\right)^2\right\} f_\alpha\left(1-f_\alpha\right) + \mathrm{Tr}\left\{tt^\dagger\left(\mathbb{1}_\alpha - tt^\dagger\right)\right\}\left[f_\alpha + f_\beta - 2f_\alpha f_\beta\right]\Big)\mathrm{d}\epsilon \tag{C.4}$$

$$P_{\alpha\alpha}(\omega=0) = \frac{2e^2}{h}\int_0^\infty \mathrm{d}\epsilon\ \Big\{\mathrm{Tr}\left(tt^\dagger\right)\left[f_\alpha(1-f_\alpha) + f_\beta(1-f_\beta)\right] + \mathrm{Tr}\left\{tt^\dagger(\mathbb{1}_\alpha - tt^\dagger)\right\}\left[f_\alpha(1-f_\beta) + f_\beta(1-f_\alpha)\right]\Big\} \tag{C.5}$$

C.2.2 Case II: $\alpha \neq \beta$

We refer to (A.3) and realize that now,

$$\begin{aligned}
\text{Term(i)} =& 0 \\
\text{Term(ii)} + \text{Term(iii)} =& -\text{Tr}\left(tt^\dagger\right)\left[f_\alpha(1-f_\alpha) + f_\beta(1-f_\beta)\right] \\
\text{Term(iv)} =& f_\alpha(1-f_\beta)\ \text{Tr}\left(S^\dagger_{\alpha\alpha}S_{\alpha\beta}S^\dagger_{\beta\beta}S_{\beta\alpha}\right) \\
&+ f_\beta(1-f_\alpha)\ \text{Tr}\left(S^\dagger_{\alpha\beta}S_{\alpha\alpha}S^\dagger_{\beta\alpha}S_{\beta\beta}\right) \\
&+ \underbrace{f_\alpha(1-f_\alpha)\ \text{Tr}\left(S^\dagger_{\alpha\alpha}S_{\alpha\alpha}S^\dagger_{\beta\alpha}S_{\beta\alpha}\right)}_{a} \\
&+ \underbrace{f_\beta(1-f_\beta)\ \text{Tr}\left(S^\dagger_{\alpha\beta}S_{\alpha\beta}S^\dagger_{\beta\beta}S_{\beta\beta}\right)}_{b}
\end{aligned}$$

A close analysis of Term(iv) tells us that, expansion of $(\text{Term(iv}_\text{a}) + \text{Term(iv}_\text{b}))$, cancels with $(\text{Term(ii)} + \text{Term(iii)})$, thus finally giving us,

$$\begin{aligned}
P_{\alpha\beta}(\omega=0) = -\int_0^\infty \Big(&\text{Tr}\left\{\left(tt^\dagger\right)^2\right\} f_\beta\left(1-f_\beta\right) + \text{Tr}\left\{\left(t't'^\dagger\right)^2\right\} f_\alpha\left(1-f_\alpha\right) \\
&+\text{Tr}\left\{t't'^\dagger\left(\mathbb{1}_\beta - t't'^\dagger\right)\right\}\left[f_\alpha + f_\beta - 2f_\alpha f_\beta\right]\Big)\mathrm{d}\epsilon
\end{aligned} \tag{C.6}$$

Now, only in presence of time reversal symmetry, we can obtain the following by comparing (C.4) and (C.6),

$$\boxed{P_{\alpha\beta}(\omega=0) = -P_{\alpha\alpha}(\omega=0)} \tag{C.7}$$

Appendix D

Analysing noise in presence of a temperature difference ($\Theta \neq 0$)

As derived in Appendix C,

$$P_{\alpha\alpha}(\omega=0) = \int_0^\infty \Big(\mathrm{Tr}\left\{ \left(tt^\dagger\right)^2 \right\} f_\beta \left(1-f_\beta\right) + \mathrm{Tr}\left\{ \left(t't'^\dagger\right)^2 \right\} f_\alpha \left(1-f_\alpha\right) + \mathrm{Tr}\left\{ tt^\dagger \left(\mathbb{1}_\alpha - tt^\dagger\right) \right\} \left[f_\alpha + f_\beta - 2 f_\alpha f_\beta \right] \Big) \mathrm{d}\epsilon \tag{D.1}$$

$$P_{\alpha\beta}(\omega=0) = -\int_0^\infty \Big(\mathrm{Tr}\left\{ \left(tt^\dagger\right)^2 \right\} f_\beta \left(1-f_\beta\right) + \mathrm{Tr}\left\{ \left(t't'^\dagger\right)^2 \right\} f_\alpha \left(1-f_\alpha\right) + \mathrm{Tr}\left\{ t't'^\dagger \left(\mathbb{1}_\beta - t't'^\dagger\right) \right\} \left[f_\alpha + f_\beta - 2 f_\alpha f_\beta \right] \Big) \mathrm{d}\epsilon \tag{D.2}$$

Let me define,

$$\mathrm{Tr}\left\{\left(tt^{\dagger}\right)^{2}\right\} = h_1(\epsilon) \quad \text{and} \mathrm{Tr}\left\{\left(t't'^{\dagger}\right)^{2}\right\} = h_2(\epsilon)$$
$$\mathrm{Tr}\left\{tt^{\dagger}\left(\mathbb{1}_{\alpha} - tt^{\dagger}\right)\right\} = (g_1(\epsilon) - h_1(\epsilon))$$
$$\mathrm{Tr}\left\{t't'^{\dagger}\left(\mathbb{1}_{\beta} - t't'^{\dagger}\right)\right\} = (g_2(\epsilon) - h_2(\epsilon))$$

Let me write 1 for the αth lead and 2 for the βth lead. Under time reversal symmetry, we can drop the lead indices and write,

When $\Theta = 0$, the current noise power is given by,

$$P = \frac{2e^2}{h}\sum_{n}\int_{0}^{\infty} d\epsilon \left[\Big(f_1 + f_2\Big)T_n - 2T_n\Big(1 - T_n\Big)f_1 f_2 - \Big(f_1^2 + f_2^2\Big)T_n^2\right], \quad \text{(D.3)}$$

where,

f_1, f_2: Fermi distribution functions of electrons in leads 1 (left) or 2(R) (right), respectively.

$$f_{1(2)} = \frac{1}{e^{\beta_{1(2)}(\epsilon - \mu_{1(2)})} + 1}.$$

T_n: Transmission function of the nth channel; in general it is a function of energy (ϵ).

Let us assume that the transmission function is a flat function of energy, so that, $T_n(\epsilon) = T_n(\epsilon_F)$, and can be taken out of the energy integral.

$$P(V,T) = \frac{2e^2}{h}\sum_n \Bigg[T_n \underbrace{\int_0^\infty d\epsilon \Big(f_1 + f_2\Big)}_{I_1} - 2T_n\Big(1-T_n\Big)\underbrace{\int_0^\infty d\epsilon \;\; f_1 f_2}_{I_2} - T_n^2 \underbrace{\int_0^\infty d\epsilon \Big(f_1^2 + f_2^2\Big)}_{I_3}\Bigg]. \tag{D.4}$$

The above equation can be exactly solved to get a closed form expression, as a function of the applied bias voltage (V) and ambient temperature (T). Hence (D.3), in the limit when $e^{\beta\mu_1}$ and $e^{\beta\mu_1} >> 1$ becomes,

$$P(V,T) = I_1 - I_2 - I_3, \tag{D.5}$$

with,

$$\begin{aligned} I_1 &= \mu_1 + \mu_2, \\ I_2 &= \frac{\mu_1 e^{-\beta\mu_1} - \mu_2 e^{-\beta\mu_2}}{e^{-\beta\mu_1} - e^{-\beta\mu_2}}, \\ I_3 &= (\mu_1 + \mu_2) - \frac{2}{\beta}, \end{aligned}$$

which can be substituted in (D.3) to get,

$$P(V,T) = \frac{2e^2}{h}\sum_n \Bigg[2k_BT \;\; T_n^2 - T_n\Big(1-T_n\Big)eV\coth\frac{eV}{2k_BT}\Bigg]. \tag{D.6}$$

Now let us consider the case when $\Theta \neq 0$. Let, $T_2 = T$ and $T_1 = T + \Theta$; $\mu_2 = \mu$, and $\mu_1 = eV + \mu$. In order to be able to solve (D.3) exactly we have to do the following,

$$f_1(\epsilon, \mu_1, T_1) = \bar{f}_1(\epsilon, \mu_1, T) + \Theta\frac{\partial \bar{f}(\epsilon, \mu_1, T)}{\partial T}$$

or,

$$f_1(\epsilon, \mu_1, T_1) = \bar{f}_1(\epsilon, \mu_1, T) + \frac{\Theta}{k_B T^2} \frac{(\epsilon - \mu_1) e^{\beta(\epsilon - \mu_1)}}{[1 + e^{\beta(\epsilon - \mu_1)}]^2} \tag{D.7}$$

where,

$$\bar{f}_1(\epsilon, \mu_1, T) = \frac{1}{[1 + e^{\beta(\epsilon - \mu_1)}]},$$

and, $\beta = 1/k_B T$. If we substitute the above in (D.3) we get,

$$P(V, T, \Theta) = P_0(V, T) + \Delta P(V, T, \Theta),$$

where,

$$P_0(V, T) = \frac{2e^2}{h} \sum_n \left[2k_B T \;\; T_n^2 - T_n \Big(1 - T_n \Big) eV \coth \frac{eV}{2k_B T} \right],$$

$$\begin{aligned} \Delta P(V, T, \Theta) =& I' \\ =& \frac{\Theta}{k_B T^2} \int_0^\infty \frac{(\epsilon - \mu_1) e^{\beta(\epsilon - \mu_1)} \mathrm{d}\epsilon}{[1 + e^{\beta(\epsilon - \mu_1)}]^2 [1 + e^{\beta(\epsilon - \mu_2)}]}. \end{aligned}$$

Let us cosider the integral I':[1]

$$I' = \frac{\Theta}{T^2} \Bigg[\underbrace{\int_0^\infty \frac{(\epsilon - \mu) e^{(\epsilon - \mu - V)/T} \mathrm{d}\epsilon}{[1 + e^{-V/T} e^{(\epsilon - \mu)/T}]^2 [1 + e^{(\epsilon - \mu)/T}]}}_{I'^{(1)}} - eV \underbrace{\int_0^\infty \frac{e^{(\epsilon - \mu - V)/T} \mathrm{d}\epsilon}{[1 + e^{(\epsilon - \mu)/T} e^{-V/T}]^2 [1 + e^{(\epsilon - \mu)/T}]}}_{I'^{(2)}} \Bigg]$$

[1] I have wriiten eV as V

where, everything has written in units of k_B.

Let, $\epsilon - \mu = x$,

$$I' = \frac{\Theta}{T^2}\left[\int_{-\mu}^{\infty} \frac{(x-V)e^{(x-V)/T}\mathrm{d}x}{[1+e^{-V/T}e^{x/T}]^2[1+e^{x/T}]}\right]$$
$$\approx \frac{\Theta}{T^2}\left[\int_{-\infty}^{\infty} \frac{(x-V)e^{(x-V)/T}\mathrm{d}x}{[1+e^{-V/T}e^{x/T}]^2[1+e^{x/T}]}\right].$$

Let, $x/T = y$, then,

$$I' = \int_{-\infty}^{\infty} \frac{(y-\bar{V})e^{(y-\bar{V})/T}\mathrm{d}y}{[1+e^{-\bar{V}/T}e^{y/T}]^2[1+e^{y/T}]},$$

where, $\bar{V} = V/T$.

$\therefore$

$$I'_1 = \gamma \int_{-\infty}^{\infty} \frac{ye^y \ \mathrm{d}y}{[\gamma+e^y]^2[1+e^y]}, \tag{D.8}$$

and,

$$I'_2 = \bar{V}\gamma \int_{-\infty}^{\infty} \frac{e^y \ \mathrm{d}y}{[\gamma+e^y]^2[1+e^y]}, \tag{D.9}$$

where, $\gamma = e^{\bar{V}}$.

The above integrals can be solved exactly by the help of the following two integrals:

$$\int_{-\infty}^{\infty} \frac{y \ \mathrm{d}y}{[\gamma+e^y][1+e^y]} = \frac{(\ln\gamma)^2}{2(\gamma-1)},$$

$$\int_{-\infty}^{\infty} \frac{\mathrm{d}y}{[\gamma + e^y][1 + e^y]} = \frac{\ln \gamma}{\gamma - 1}.$$

$$\begin{aligned} I_1' =& -\gamma \frac{\partial}{\partial \gamma} \int_{-\infty}^{\infty} \frac{y \ \mathrm{d}y}{[\gamma + e^y][1 + e^y]} \\ =& \frac{e^{\bar{V}}}{2} \left[\left(\frac{\bar{V}}{e^{\bar{V}} - 1} \right)^2 - \frac{2\bar{V}}{e^{\bar{V}}(e^{\bar{V}} - 1)} \right]. \end{aligned} \tag{D.10}$$

$$\begin{aligned} I_2' =& -\bar{V} e^{\bar{V}} \frac{\partial}{\partial \gamma} \int_{-\infty}^{\infty} \frac{\mathrm{d}y}{[\gamma + e^y][1 + e^y]} \\ =& \ \bar{V} e^{\bar{V}} \left[-\frac{1}{e^{\bar{V}}(e^{\bar{V}} - 1)} + \frac{\bar{V}}{(e^{\bar{V}} - 1)} \right]. \end{aligned} \tag{D.11}$$

$\therefore$

$$I' = -\frac{1}{2} \left(\frac{\bar{V}}{2 \sinh(\bar{V}/2)} \right)^2. \tag{D.12}$$

$\therefore$

$$\Delta P(V, T, \Theta) = P_0(V, T, \Theta) + k_B \sum_n \left(\Theta \ T_n^2 + \Theta \ T_n(1 - T_n) \right) \left(\frac{\bar{V}}{2 \sinh(\bar{V}/2)} \right)^2. \tag{D.13}$$

In the linear response regime,

$$\lim_{V \to 0} \Delta P = \sum_n T_n k_B \Theta. \tag{D.14}$$

However, if time reversal symmetry does not hold, then the scattering matrix is not symmetric and hence, $t' \neq t$. In that case, $P_{\alpha\alpha} \neq P_{\alpha\beta}$ will be given by,

$$P_{\alpha\alpha} = \frac{2e^2}{h}\left[k_B T\left(h_1 + h_2\right) + k_B\theta\ \ h_2 + \left(g_1 - h_1\right)\left(eV\coth\left(\frac{eV}{k_B T}\right) + I'\right)\right] \quad \text{(D.15)}$$

$$P_{\alpha\beta} = \frac{2e^2}{h}\left[k_B T\left(h_1 + h_2\right) + k_B\theta\ \ h_2 + \left(g_2 - h_2\right)\left(eV\coth\left(\frac{eV}{k_B T}\right) + I'\right)\right] \quad \text{(D.16)}$$

where, the functions h_1, h_2, g_1, g_2, are calculated at the Fermi energy.

Appendix E

Mathematical tools to implement the Sommerfeld Expansion

E.1 List of Integrals used

$$\int \frac{\mathrm{d}x}{1+e^{-x}} = \ln(1+e^{x}) \tag{E.1}$$

$$\int \frac{\mathrm{d}x}{1+e^{x}} = -\ln(1+e^{-x}) \tag{E.2}$$

$$\int \frac{\mathrm{d}x}{(1+e^{-x})^2} = \left(\frac{-1}{1+e^{-x}}\right) + \ln(1+e^{x}) \tag{E.3}$$

$$\int \frac{\mathrm{d}x}{(1+e^{x})^2} = \left(\frac{1}{1+e^{x}}\right) - \ln(1+e^{-x}) \tag{E.4}$$

$$\int \ln(1+e^{x})\mathrm{d}x = -\mathrm{Li}_2(-e^{x}) \tag{E.5}$$

$$\int \ln(1+e^{-x})\mathrm{d}x = \mathrm{Li}_2(-e^{-x}) \tag{E.6}$$

$$\int \left(\int \ln(1+e^{x})\mathrm{d}x\right)\mathrm{d}x = -\mathrm{Li}_3(-e^{x}) \tag{E.7}$$

$$\int \left(\int \ln(1+e^{-x})\mathrm{d}x\right)\mathrm{d}x = -\mathrm{Li}_3(-e^{-x}) \tag{E.8}$$

$$\int_0^\infty \ln(1+e^{-x})\mathrm{d}x = \frac{\pi^2}{12} \tag{E.9}$$

E.2 Functional identities and particular values of the Polylogarithm function

$$\mathrm{Li}_2(-1) = -\frac{\pi^2}{12} \tag{E.10}$$

$$\mathrm{Li}_3(-1) = -\frac{3}{4}\zeta(3) \tag{E.11}$$

$$\mathrm{Li}_2(0) = 0 \tag{E.12}$$

$$\mathrm{Li}_3(0) = 0 \tag{E.13}$$

$$\mathrm{Li}_2(z) = -\mathrm{Li}_2\left(\frac{z}{z-1}\right) - \frac{1}{2}\ln^2(1-z) \;\; /; \;\; z \notin (1,\infty) \tag{E.14}$$

$$\begin{aligned}\mathrm{Li}_3(z) = &-\mathrm{Li}_3\left(\frac{z}{z-1}\right) - \mathrm{Li}_3\left(\frac{1}{1-z}\right) \\ &+ \frac{1}{3}\ln^3(1-z) - \frac{1}{2}\ln(-z)\ln^2(1-z) \\ &- \frac{1}{6}\pi^2\ln(1-z) + \zeta(3) \;\; /; \;\; z \notin (1,\infty)\end{aligned} \tag{E.15}$$

E.3 Relationship between Fermi-Dirac Integrals and Polylogarithm

The complete Fermi Dirac integral for an index j is given by,

$$F_n(x) = \frac{1}{\Gamma(n+1)}\int_0^\infty \frac{t^n}{1+\exp[t-x]}\;\mathrm{d}t \tag{E.16}$$

where,

$\Gamma(j+1)$ is the Gamma function.

$$\because F_n(x) = \int F_{n-1}\ \mathrm{d}x$$
$$\therefore F_1(x) = \int \ln(1+e^x)\ \mathrm{d}x$$

Again, by definition of the polylogarithm function,

$$\mathrm{Li}_n(\eta) = \frac{1}{\Gamma(\eta)} \int_0^\infty \frac{t^{(n-1)}}{1+\exp[t]\eta^{-1}}\ \mathrm{d}t \tag{E.17}$$

If, $\eta = -\exp[x]$, then,

$$\mathrm{Li}_n(-e^x) = -F_{n-1}(x) \tag{E.18}$$

E.4 Integrals appearing in the Sommerfeld Expansion

The following integrals are evaluated in the limit $\beta\mu >> 1$.

$$\begin{aligned}
\int_{-\beta\mu}^{\infty} \frac{xe^x}{(1+e^x)^2}\ \mathrm{d}x &= -\left[\ \frac{x}{1+e^x}\right]_{-\beta\mu}^{\infty} + \int_{-\beta\mu}^{\infty} \frac{\mathrm{d}x}{1+e^x} \\
&= -\left[\ \frac{x}{1+e^x} + \ln(1+e^{-x})\right]_{-\beta\mu}^{\infty} \\
&= [-\beta\mu + \beta\mu] \\
&= 0
\end{aligned}$$

$$\boxed{I_1 = \int_{-\beta\mu}^{\infty} \frac{xe^x}{(1+e^x)^2}\ \mathrm{d}x = 0} \tag{E.19}$$

$$\boxed{I_2 = \int_{-\infty}^{\infty} \frac{x^2e^x}{(1+e^x)^2}\ \mathrm{d}x = 2\zeta(2) = \frac{\pi^2}{3}} \tag{E.20}$$

$$
\begin{aligned}
\int_{-\beta\mu}^{\infty} \frac{xe^x}{(1+e^x)^3}\ \mathrm{d}x &= -\int_{0}^{\beta\mu} \frac{xe^{-x}}{(1+e^{-x})^3}\ \mathrm{d}x + \int_{0}^{\infty} \frac{xe^x}{(1+e^x)^3}\ \mathrm{d}x \\
&= -\ \frac{1}{2}\left(\left[\frac{x}{(1+e^{-x})^2} \right]_0^{\beta\mu} - \int_0^{\beta\mu} \frac{\mathrm{d}x}{(1+e^x)^2} \right) \\
&\quad + \frac{1}{2}\left[-\ \frac{x}{(1+e^x)^2} + \int_0^{\infty} \frac{\mathrm{d}x}{(1+e^x)^2} \right] \\
&= -\ \frac{1}{2}\left[\frac{x}{(1+e^{-x})^2} + \frac{1}{1+e^{-x}} - \ln(1+e^x) \right]_0^{\beta\mu} \\
&\quad + \frac{1}{2}\left[\frac{-x}{(1+e^x)^2} + \frac{1}{1+e^x} - \ln(1+e^{-x}) \right]_0^{\infty} \\
&= -\frac{1}{2}
\end{aligned}
$$

$$
\therefore \boxed{I_3 = \int_{-\beta\mu}^{\infty} \frac{xe^x}{(1+e^x)^3}\ \mathrm{d}x = -\frac{1}{2}} \tag{E.21}
$$

$$
\begin{aligned}
\int_{-\beta\mu}^{\infty} \frac{x^2e^x}{(1+e^x)^3}\ \mathrm{d}x &= \int_{0}^{\beta\mu} \frac{x^2e^{-x}}{(1+e^{-x})^3}\ \mathrm{d}x + \int_{0}^{\infty} \frac{x^2e^x}{(1+e^x)^3}\ \mathrm{d}x \\
&= \frac{1}{2}\left[\ \frac{x^2}{(1+e^{-x})^2} \right]_0^{\beta\mu} - \int_0^{\beta\mu} \frac{x}{(1+e^{-x})^2}\mathrm{d}x \\
&\quad + \frac{1}{2}\left[-\ \frac{x^2}{(1+e^x)^2} \right]_0^{\infty} + \int_0^{\infty} \frac{x}{(1+e^x)^2}\mathrm{d}x \\
&= \left[\frac{1}{2}\ \frac{x^2}{(1+e^{-x})^2} - (x+1)\ln(1+e^x) + \frac{x}{1+e^{-x}} - \mathrm{Li}_2(-e^x) \right]_0^{\beta\mu} \\
&\quad + \left[\frac{1}{2}\ \frac{x^2}{(1+e^x)^2} + (1-x)\ln(1+e^{-x}) + \frac{x}{1+e^x} + \mathrm{Li}_2(-e^{-x}) \right]_0^{\infty} \\
&= \left(\frac{\pi^2}{12} + \ln 2 \right) + \left(\frac{\pi^2}{12} - \ln 2 \right) = \frac{\pi^2}{6}
\end{aligned}
$$

$$\therefore \boxed{I_4 = \int\limits_{-\beta\mu}^{\infty} \frac{x^2 e^x}{(1+e^x)^3}\ \mathrm{d}x = \frac{\pi^2}{6}} \tag{E.22}$$

$$\begin{aligned}
\int\limits_{-\beta\mu}^{\infty} \frac{x^3 e^x}{(1+e^x)^3}\ \mathrm{d}x &= -\int\limits_{0}^{\beta\mu} \frac{x^3 e^{-x}}{(1+e^{-x})^3}\ \mathrm{d}x + \int\limits_{0}^{\infty} \frac{x^3 e^x}{(1+e^x)^3}\ \mathrm{d}x \\
&= -\ \frac{1}{2}\left[\frac{x^3}{(1+e^{-x})^2}\right]_0^{\beta\mu} + \frac{3}{2}\int\limits_{0}^{\beta\mu} \frac{x^2}{(1+e^{-x})^2}\ \mathrm{d}x \\
&\quad + \frac{3}{2}\int\limits_{0}^{\infty} \frac{x^2}{(1+e^x)^2}\ \mathrm{d}x \\
&= -\frac{1}{2}\Bigg[\frac{x^3}{(1+e^{-x})^2} + \frac{3x^2}{1+e^{-x}} - 3x(x+2)\ln(1+e^x) \\
&\quad -6(x+1)\mathrm{Li}_2(-e^x) + 6\mathrm{Li}_3(-e^x)\Bigg]_0^{\beta\mu} \\
&\quad +3\int\limits_{0}^{\infty} x\ln(1+e^{-x})\mathrm{d}x - 3\int\limits_{0}^{\infty} \frac{x}{1+e^x}\mathrm{d}x \\
&= -\left[\frac{\pi^2}{2} + \frac{21}{8}\zeta(3) + \frac{9}{4}\zeta(3)\right] + \left[\frac{9}{4}\zeta(3) - \frac{\pi^2}{4}\right] \\
&= -\ \frac{3}{4}\left(\pi^2 + \frac{7}{2}\zeta(3)\right)
\end{aligned}$$

$$\therefore \boxed{I_5 = \int\limits_{-\beta\mu}^{\infty} \frac{x^3 e^x}{(1+e^x)^3}\ \mathrm{d}x = -\ \frac{3}{4}\left(\pi^2 + \frac{7}{2}\zeta(3)\right) = C}$$

E.5 Use of Sommerfeld Expansion:

We need to evaluate an expression that looks like the following:

$$S = \int\limits_{0}^{\infty} g(\epsilon)\Big[f_1(\epsilon)+f_2(\epsilon)\Big]\mathrm{d}\epsilon - 2\int\limits_{0}^{\infty}\Big[g(\epsilon)-h(\epsilon)\Big]f_1(\epsilon)f_2(\epsilon)\mathrm{d}\epsilon - \int\limits_{0}^{\infty} h(\epsilon)\Big[f_1^2(\epsilon)+f_2^2(\epsilon)\Big]\mathrm{d}\epsilon \tag{E.23}$$

where,

$$\int k(\epsilon)\mathrm{d}\epsilon = K(\epsilon)$$

I will also use the fact that,

- $eV << \mu_1$ or μ_2
- $T_1 = T_2 + \theta$ but $\theta << T$

Now let us proceed towards evaluating the following integrals using Sommerfeld expansion,

1. $\int_0^\infty k(\epsilon)\left[f_1(\epsilon) + f_2(\epsilon)\right]\mathrm{d}\epsilon$

$$\begin{aligned}
\int_0^\infty k(\epsilon) f_1(\epsilon)\mathrm{d}\epsilon &= -K(0) + \int_0^\infty \left(-\frac{\partial f}{\partial \epsilon}\right) K(\epsilon)\mathrm{d}\epsilon \\
&= -K(0) + K(\mu_1) + \frac{k'(\mu_1)}{2\beta_1^2} I_2 \\
&= -K(0) + K(\mu_1) + \frac{k'(\mu_1)}{\beta_1^2}\ \frac{\pi^2}{6} \\
&= -K(0) + K(\mu) + eVg(\mu) + \frac{\pi^2}{6}\left[\frac{k'(\mu)}{\beta^2} + \frac{eVk''}{\beta^2}\right]\left(1 + \frac{2\theta}{T}\right) \\
\int_0^\infty k(\epsilon) f_2(\epsilon) &= -K(0) + K(\mu_2) + \frac{k'(\mu_2)}{\beta_2^2}\frac{\pi^2}{6}
\end{aligned}$$

$$\begin{aligned}
\int_0^\infty k(\epsilon)\left[f_1(\epsilon) + f_2(\epsilon)\right] = &-2K(0) + 2\left(K + \frac{k'\pi^2}{6\beta^2}\right) + eV\left(k + \frac{k''\pi^2}{6\beta^2}\right) \\
&+ \frac{k'\pi^2}{3\beta^2}\ \frac{\theta}{T} + \frac{k''\pi^2}{3\beta^2}\ \frac{eV\theta}{T}
\end{aligned} \tag{E.24}$$

2.

$$\begin{aligned}\int_0^\infty k(\epsilon) f_1^2(\epsilon) \mathrm{d}\epsilon =& - K(0) + K(\mu_1) + \frac{2k(\mu_1)}{\beta_1} I_3 + \frac{k'(\mu_1)}{\beta_1^2} I_4 \\ =& - K(0) + K(\mu_1) - \frac{k(\mu_1)}{\beta_1} + \frac{k'(\mu_1)}{\beta_1^2} \ \frac{\pi^2}{6} \\ =& - K(0) + \left(K - \frac{k}{\beta} + \frac{k'}{\beta^2} \ \frac{\pi^2}{6} \right) \\ & + eV \left(k - \frac{k'}{\beta} + \frac{k}{\beta^2} \ \frac{\pi^2}{6} \right) \\ & + \frac{\theta}{T} \left(\frac{k'}{\beta^2} \ \frac{\pi^2}{3} - \frac{k}{\beta} \right) + \frac{eV\theta}{T} \left(\frac{k''}{\beta^2} \ \frac{\pi^2}{3} - \frac{k'}{\beta} \right)\end{aligned}$$

$$\therefore \int_0^\infty k(\epsilon) \left(f_1(\epsilon) - f_1^2(\epsilon) \right) \mathrm{d}\epsilon = \frac{k(\mu_1)}{\beta_1} \tag{E.25}$$

$$= \left(\frac{k(\mu) + eVk'(\mu)}{\beta} \right) \left(1 + \frac{\theta}{T} \right) \tag{E.26}$$

$$\int_0^\infty k(\epsilon) \left(f_2(\epsilon) - f_2^2(\epsilon) \right) \mathrm{d}\epsilon = \frac{k(\mu)}{\beta} \tag{E.27}$$

3. $2 \int_0^\infty k(\epsilon) f_1(\epsilon) f_2(\epsilon) \mathrm{d}\epsilon$

In order to be able to evaluate this integral analytically I used,

$$f_1(\epsilon) = f(\epsilon) + eV \left(-\frac{\partial f}{\partial \epsilon} \right) + \frac{\theta}{T} (\epsilon - \mu) \left(-\frac{\partial f}{\partial \epsilon} \right)$$

Now,

$$\begin{aligned}\int_0^\infty k(\epsilon) f_1(\epsilon) f_2(\epsilon) \mathrm{d}\epsilon =& \int_0^\infty k(\epsilon) f^2(\epsilon) \mathrm{d}\epsilon + \frac{eV}{2} \int_0^\infty k(\epsilon) \left(-\frac{\partial f^2}{\partial \epsilon} \right) \mathrm{d}\epsilon \\ & + \frac{\theta}{2T} \int_0^\infty (\epsilon - \mu) \left(-\frac{\partial f^2}{\partial \epsilon} \right) k(\epsilon) \mathrm{d}\epsilon\end{aligned}$$

A similar treatment as before gives us,

$$\int_0^\infty k(\epsilon) f^2(\epsilon) \mathrm{d}\epsilon = K - \frac{k}{\beta} + \frac{k'}{\beta^2} \ \frac{\pi^2}{6} - K(0) \tag{E.28}$$

$$\frac{eV}{2} \int_0^\infty k(\epsilon) \left(-\frac{\partial f^2}{\partial \epsilon} \right) \mathrm{d}\epsilon = \frac{eV}{2} \left[k - \frac{k'}{\beta} + \frac{k''}{\beta^2} \ \frac{\pi^2}{6} \right] \tag{E.29}$$

$$\frac{\theta}{2T} \int_0^\infty (\epsilon - \mu) \left(-\frac{\partial f^2}{\partial \epsilon} \right) k(\epsilon) \mathrm{d}\epsilon = \frac{\theta}{2T} \left[-\frac{k}{\beta} + \frac{k'}{\beta^2} \ \frac{\pi^2}{3} + \frac{k''}{\beta^3} C \right] \tag{E.30}$$

Collecting all the terms,

$$\begin{aligned} 2 \int_0^\infty k(\epsilon) f_1(\epsilon) f_2(\epsilon) \mathrm{d}\epsilon = \ & 2 \left(K - \frac{k}{\beta} + \frac{k'}{\beta^2} \ \frac{\pi^2}{6} \right) \\ & + eV \left(k - \frac{k'}{\beta} + \frac{k''}{\beta^2} \ \frac{\pi^2}{6} \right) \\ & + \frac{\theta}{T} \left(-\frac{k}{\beta} + \frac{k'}{\beta^2} \ \frac{\pi^2}{3} + \frac{k''}{\beta^3} C \right) - 2K(0) \end{aligned} \tag{E.31}$$

$$\begin{aligned} \int_0^\infty k(\epsilon) \left(f_1 + f_2 \right) \mathrm{d}\epsilon = & -2K(0) + 2 \left(K + \frac{k' \pi^2}{6\beta^2} \right) + eV \left(k + \frac{k'' \pi^2}{6\beta^2} \right) \\ & + \frac{k' \pi^2}{3\beta^2} \ \frac{\theta}{T} + \frac{k'' \pi^2}{3\beta^2} \ \frac{eV\theta}{T} \end{aligned} \tag{E.32}$$

Subtracting (E.31) from (E.32), I get,

$$\mathrm{term}_1 = 2\frac{k}{\beta} + eV\frac{k'}{\beta} + \frac{\theta}{T} \left(\frac{k}{\beta} - \frac{k''}{\beta^3} C \right) + \frac{eV\theta}{T} \ \frac{k'' \pi^2}{3\beta^2} \tag{E.33}$$

Bibliography

[1] Slinker *et. al.*, New J. Phys. **7**, 246 (2005).

[2] S. Nadj-Perge *et. al.*, Nature (London) **468**, 1024 (2010).

[3] Landauer, R., IBM J. Res. Dev. **1**, 223 (1957).

[4] van Wees *et al.*, Phys. Rev. Lett. **60**, 848 (1988).

[5] M. A. Kastner *et al.*, AIP Conference Proceedings, no. **275**, 573-851 (1993).

[6] E. B. Foxman *et al.*, Phys. Rev. B **47**, 10020 (1993).

[7] D. Dixon *et al.*, Surf. Sci., **361-362**, 636-9 (1996).

[8] Koester *et al.*, Phys. Rev. B **53**, 13063 (1996).

[9] Todorov, T.N., Phil. Mag. B **77**, 965 (1998).

[10] Giazotto *et al.*, Rev. Mod. Phys. **78**, 27 (2007).

[11] Saira *et al.*, Phys. Rev. Lett. **99**, 027203 (2007).

[12] C. T. White and Todorov, Nature **393**, 240 (1998).

[13] Th. Martin and R. Landauer, Phys. Rev. B **45**, 4 (1992).

[14] Ya. M. Blanter and M. Buttiker, Physics Reports **336**, 1-2 (2000).

[15] P. N. Butcher, J. Phys. Cond. Matt. **2**, 4869 (1990).

[16] L. V. Krive *et al.*, Phys. Rev. B **64**, 233304 (2001).

[17] C. Beenakker and Schönenberger, Physics Today, page 37, may 2003.

[18] Jong and Beenakker, arXiv:cond-mat/9611140v1 (1996)

[19] M Büttiker, Phys. Rev. B **41**, 7906 (1990).

[20] R. Landauer, Phys. Rev. B **47**, 16427 (1993).

[21] M. B. Johnson, Phys. Rev. **29**, 367 (1927).

[22] H. Nyquist, Phys. Rev. **32**, 110 (1928).

[23] G. B. Lesovik, JETP Lett. **49**, 592 (1989).

[24] E. V. sukhorokov and D. Loss, Phys. Rev. B **59**, 13054 (1999).

[25] *'Introduction to Mesoscopic Physics'*, Oxford University Press, Y. Imry.

[26] *'Electrical Transport in Nanoscale systems'*, Cambridge University Press, M. Di Ventra

[27] *'Electronic Noise and Fluctuations in Solids*, Cambridge University Press, Sh. Kogan.

[28] *'Solid State Physics'*, Thomson (Brooks/Cole) (Indian Edition), Ashcroft and Mermin.

[29] T. Ando, Phys. Rev. B **44**, 15 (1991).

[30] Petr A. Khomyakov and Geert Brocks, Phys. Rev. B **70**, 195402 (2004).

[31] L. Molinari, J. Phys. A **30**, 983 (1997).

[32] T. N. Todorov *et. al.*, J. Phys. Cond. Matt. **5**, 2389 (1993).

[33] K. Nicolic *et. al.*, Phys. Rev. B **50**, 11008 (1994).

[34] M. P. Samanta *et. al.*, Phys. Rev. B **53**, R7626 (1996).

[35] E. G. Emberly and G. Kirczenow, Phys. Rev. B **58**, 10911 (1998).

[36] K. Hirose and M. Tsukada, Phys. Rev. Lett. **73**, 150 (1994).

[37] K. Hirose and M. Tsukada, Phys. Rev. B **51**, 5278 (1995).

[38] N. D. Lang, Phys. Rev. B **52**, 5335 (1995).

[39] N. D. Lang, Phys. Rev. Lett. **79**, 1357 (1997).

[40] M Di Ventra *et. al.*, Phys. Rev. Lett. **84**, 979 (2000).

[41] *'Electronic Transport in Mesoscopic systems'*, Cambridge University Press, S. Datta.

[42] Kristian Molhave *et al.*, Nano Lett. **6**, 8 (2006).

[43] K. A. Dean *et al.*, Appl. Phys. Lett. **79**, 1873 (2001).

[44] Todorov, T.N., Phil. Mag. B **77**, 965 (1998).

[45] M. J. Montgomery, T. N. Todorov and A. P. Sutton, J. Phys. Cond. Matt. **14**, 5377 (2002).

[46] D' Agosta, R., N. sai, and M. Di Ventra, Nano Lett. **6**, 2935 (2006).

[47] Chen, Y *et al.*, Nano Lett. **3**, 1961 (2003).

[48] Chen, Y *et al.*, Nano Lett. **4**, 1709 (2004).

[49] Chen, Y *et al.*, Nano Lett. **5**, 621 (2005).

[50] Huang, Z. F. *et al.*, Nano Lett. **6**, 1240 (2006).

[51] Conti, S., Vignale, G, Phys. Rev. B **60**, 7966 (1999).

[52] Djukic, D., van Ruitenbeek, J. M., Nano Lett., **6**, 789 (2006).

[53] Cahill *et al.*, Appl. Phys. Reviews **93**, 2 (2003).

[54] Glatz *et al.*, Phys. Rev. B **82**, 075314 (2010).

[55] R. Ward *et al.*, Nature Nanotechnology **6**, 33 (2010).

[56] Sayer *et al.*, IEEE Transcations on Components and Packaging Technologies **33**, 1 (2010).

[57] T. N. Todorov, J. Hoekstra and A. P. Sutton, Phys. Rev. Lett. **86**, 16 (2001).

[58] Todorov *et al.*, J. Phys. Cond. Matt. **16**, 3609 (2004).

[59] A. P. Horsefeld *et al.*, J. Phys. Cond. Matt. **16**, 8251 (2009).

[60] A. I. Yanson *et al.*, Nature (London) **395**, 783 (1998).

[61] H. Yasuda and A. Sakai, Phys. Rev. B **56**, 1069 (1997).

[62] K. Itakura *et al.*, Phys. Rev. B **60**, 11163 (1999).

[63] K. Hansen, PhD. thesis, University of Aarhus, 2000.

[64] Galperin *et al.*, Phys. Rev. Lett. **75**, 155312 (2007).